ATLSS Reports   Civil and Environmental Engineering

8-1-2007

Web Cracking Repair Design for Bridge SR 46-3020-00200000 on US 202 in Montgomery County, PA

Sougata Roy

Ben Yen

C. Bowman

Follow this and additional works at: http://preserve.lehigh.edu/engr-civil-environmental-atlss-reports

Web Cracking Repair Design for Bridge SR 46-3020-0020-0000 on US 202 in Montgomery County, PA

PennDOT ECMS No. E00511: Work Order No. 10

Field Instrumentation, Monitoring and Analysis

Final Report

by

Sougata Roy

Ben T. Yen

Carl A. Bowman

ATLSS Report No. 07-10

August 2007

Web Cracking Repair Design for Bridge SR 46-3020-0020-0000 on US 202 in Montgomery County, PA

PennDOT ECMS No. E00511: Work Order No. 10

Field Instrumentation, Monitoring and Analysis

Final Report

by

Sougata Roy, Ph.D.
Research Scientist, ATLSS Center

Ben T. Yen, Ph.D.
Professor Emeritus of Civil Engineering, Lehigh University

Carl A. Bowman
Instrumentation Technician, ATLSS Center

ATLSS Report No. 07-10
August 2007

ACKNOWLEDGEMENTS

CONTENTS

TABLES

FIGURES

EXECUTIVE SUMMARY

The bridge SR 46-3020-0020-0000 in Montgomery County, PA, carries new US Route 202. During the painter's inspection of a completed paint job in late August 2006, a crack was detected in the web of Girder 3 in the North Bound Span 2 at the intersection with the floor beam, above the seating for Span 1. The bridge was last inspected on April 22, 2005 by DMJM Harris and no crack was detected. In May 2006 the deck joint at this pier was replaced.

Subsequently, a field study of web cracking at Pier 1 was conducted by the ATLSS Center, Lehigh University to assess the cause of cracking and to recommend retrofit strategies. An instrumentation plan was developed to capture the behavior of the structure at the areas of high stress concentration and secondary stresses. Controlled load tests were conducted to assess the behavior of the bridge under a known vehicle weight. The stresses at the critical locations in Girder 1 were monitored for a period of about 30 days. Forensic examinations were conducted on the fracture surface to determine the nature of crack growth. The findings of the fractographic studies wee further verified by additional material tests. Mechanical properties of the girder web material, including both the tensile strength and the fracture toughness was determined, and a chemical analysis was performed. Limited Finite Element Analyses were conducted to verify the field measurements.

The investigations revealed that the cracking of the web of Girder 3 was due to cleavage fracture that probably initiated from a flaw condition at the termination of the transverse stiffener to web weld near the cope, during an unusually extreme load event, such as low temperature and/or impact from overloading. The flaw condition could be due to a relatively large weld fabrication defect or propagation of fatigue crack from micro discontinuities. To prevent cracking at similar locations in other girders, it was recommended to drill 2 in diameter holes on either side of the floor beam connection plate/bearing stiffener and just above the longitudinal weld between the bracket shelf plate and the web of the girders.

Based on the limited field monitoring data, controlled load test results and the FEA results near the bracket shelf plate in Girder 1, there should not be any concern for fatigue cracking leading to unstable fracture in the girders of Span 2 near the Pier 1, after the preventive holes are drilled. The live load stresses measured in Girder 1, near the geometrically similar cracked corner of Girder 3, was less than 1.5 ksi, which is unlikely to promote fatigue crack propagation. The fracture toughness of the web steel is about 30 ft-lb at 40^0 F in the longitudinal direction, which is more than the required 25 ft-lb at 40^0 F for Fracture-Critical Members in Zone 2, as per the current AASHTO Bridge Design Specification. The cracking in Girder 3 was an unusual event, which was probably initiated by the combination of an extreme event/constraint and the low material fracture toughness in the transverse direction (in the depth direction) of the web (about 13 ft-lb at 40^0 F). Any possible unstable cracking in the girder webs, from the junction of floor beam connection plate, bearing stiffener and the shelf plate, should be arrested by the holes drilled on either side of the connection.

1. INTRODUCTION

1.1 Background

The bridge SR 46-3020-0020-0000 carrying new US 202 in Montgomery County, PA, consists of two adjacent four span structures carrying two lanes of North Bound (NB) and South Bound (SB) traffic each. Each structure comprises two steel girder floor beam stringer system and concrete deck composite construction. During the painter's inspection of a completed paint job in late August 2006, a crack was detected in the web of Girder 3 in the North Bound Span 2 at the intersection with the floor beam, above the seating for Span 1 (Figure 1). The bridge was last inspected on April 22, 2005 by DMJM Harris [Load Case 1 –] and no crack was detected. In May 2006 the deck joint at this pier was replaced [Load Case 2 –].

Subsequent to discovery of the crack, the ATLSS Center, Lehigh University was hired in October 2006, as a subconsultant to prime HDR Engineer, Inc. through PennDOT Open End Agreement E00511: Work Order No. 10: Lehigh Master Subconsultant Agreement Task Order No. 8, for conducting field study of web cracking at Pier 1 to assess the cause of cracking and to recommend retrofit strategies. The findings of the investigations carried out according to the Task Order are reported herein.

The SR 46-3020 Bridge comprises two adjacent structures carrying two lanes of North Bound (NB) and South Bound (SB) traffic each. The Span 1 is simply supported on an abutment at the south end, and on a bracket projected from the main girders of Span 2 at the north end (Figure 2). This span over existing Reading Co. railway track is 71 ft long between expansion joints and is supported by roller and rocker bearings at the south and the north ends respectively. The Spans 2, 3, and 4 are of continuous configuration (Figure 3) having span lengths of 150 ft, 196 ft and 150 ft respectively between center lines of bearings/expansion joints. The spans are supported on rocker bearings at Pier 2 and roller bearings at other piers. They span across the Ross Road, the Crow Creek and the LR 1135 respectively. In plan the bridge deck consists of straight crossing with skew ends. The skew angle at the South Abutment and Pier 1 is 54^0, and that at the other piers/abutment is $5^015'$. The plan of the bridge is shown in Figure 4.

The deck top framing plan of Span 2 is shown in Figure 5. At Pier 1, the ends of bracket projection of main girders supporting Span 1 are connected in the transverse direction by a cross girder aligned parallel to the skew end. At the center line of bearings, the girders are connected in the transverse direction by floor beams, which are also parallel to the skew end. Thus, at Pier 1 the Girder 1 (the SB exterior girder) and Girder 3 (the NB interior girder) of Span 2 form acute corners with the floor beams, while the other two girders subtend obtuse angles.

The bearing stiffeners and the girder floor beam connection plates at Pier 1 are interrupted by the top flange of the bracket projections extending into the girder webs (Figures 7 and 11). The bracket flange plates are welded all around to the web. The bearing stiffeners are milled to bear against the bracket flange plates (Figure 9). A cope of about 1in × 1 in is provided in the bearing stiffeners for uninterrupted passage of the bracket flange to web weld. The floor beam connection plates and other transverse stiffeners have been stopped short of the bearing shelf plate by about 1 in (Figure 10).

1.2 Scope of Work

Per the original task order, Lehigh's scope of work was as follows:

(i) Develop instrumentation plan to capture the behavior of the structure at the areas of high stress concentration and secondary stresses.

(ii) Conduct crawl and dynamic load tests to assess the overall behavior of the bridge in its current condition under a known vehicle weight.

(iii) Conduct short term monitoring for one week to obtain an indication of the response under random traffic and an understanding of the cause of cracking.

(iv) Conduct finite element analysis of the structure to determine the areas of critical stress concentrations and to assess the anticipated performance of potential retrofit concepts. Calibrate finite element model using the field data obtained during the controlled load test.

(v) Prepare interim report summarizing the instrumentation plan; the findings of controlled load tests, finite element analyses, and short term monitoring; and the development of retrofit concepts.

(vi) Conduct long term monitoring for 30 days to evaluate the effectiveness of the proposed retrofit after the repairs have been implemented.

(vii) Prepare final report including the findings of the interim report along with the findings from the long-term monitoring evaluating the performance of the retrofitted structure.

During execution of the task order, however, it was determined that an elaborate retrofit of the bridge is not required due to the unusually small stresses experienced by the critical details. Fractographic examinations were carried out to determine the source of cracking, which revealed crack growth from brittle fracture. To confirm this finding material testing of the girder web steel was conducted. Both the fractographic examinations and the material studies were not included in the original scope of work, which was redefined in view of the findings of the controlled load test and additional forensic investigations. The scope of finite element analyses as identified in item (iv) above was curtailed and the long term monitoring in item (vi) was eliminated in lieu of the fractographic and material studies.

1.3 Approach

To accomplish the scope of work, following methodology was adopted:

(i) A field inspection of the bridge was conducted to familiarize with the field and the bridge condition, to determine the extent of cracking, and to identify other potential cracking locations similar to the cracked girder.

(ii) To determine the stress condition that may have initiated the cracking in Girder 3, stresses near the geometrically similar corner of Girder 1 were measured under controlled loads and were monitored for a period of 30 days under in-service traffic.

(iii) An instrumentation plan was developed employing 35 data channels that included 17 axial strain gages, four strain rosettes, and four LVDTs.

(iv)   Forensic examinations were conducted on the fracture surface to determine the nature of crack growth.

(v)   Mechanical properties of the girder web material were examined to determine the reason of cracking. Both tensile strength and fracture toughness of the material was determined

(vi)   Chemical composition of the cracked web plate was determined to verify the material type and properties.

(vii)   Based on the findings retrofit measures were recommended.

1.4   Field View

Pursuant to the Notice to Proceed (NTP), a field view of the bridge was carried out on 10/10/2006. The inspection was limited to the end of the girders in Span 2 at Pier 1, particularly of the web area near the seat for Span 1 (Figure 11).

During the field inspection it was noted that the flange and web of the girders near this end was corroded from road salt drip through the deck expansion joint above. These corrosion products packed the cope hole in the bearing stiffeners and reduced the size of the opening.

The cracks in Girder 3 had initiated from the cope in the transverse bearing stiffener near the termination of the bearing stiffener/floor beam connection plate-to-web weld above the bracket shelf plate (Figures 12 and 13). The crack then propagated diagonally into the web on both sides of the stiffener/connection plate. Towards the end of the girder the crack completely fractured the girder web (Figure 1). On the other direction, the crack terminated after growing for about three inches. Further possible growth into the web was arrested by drilling holes at the crack tip. Except at Girder 3 (the NB interior girder), no cracking was observed in any of the other girders.

The Pier 1 and the underside of Span 2 were easily accessible via Ross Road which had moderate local traffic. The railway track under Span 1 was scarcely traversed and had safe clearance from the Pier 1. It was determined that the underside of Span 2 deck could be easily accessed by a manlift, with minimum traffic control (Figure 15). The top of barrier wall at Pier 1 provided sufficient space for safe storage of field instrumentation and monitoring equipments.

2.   INSTRUMENTATION PLAN

The instrumentation plan is shown in Figures 16, 17 and 18. Same instrumentation was provided for both the controlled load tests and the short term monitoring. Altogether 35 data channels were employed for 17 axial strain gages, four strain rosettes, and four LVDTs. The instruments were installed on November 13 and 14, 2006 during the day time.

2.1   Selection of Instrumentation Location

Since the Girder 3 was cracked, the local stress field was changed from the un-cracked state and as such it was realized that the instrumentation of this girder would not provide the stress condition that may have initiated the cracking. Accordingly, it was decided to measure stresses and displacements at the geometrically similar corner of Girder 1, which was un-cracked. It may be noted that the Girder 3 (the NB interior girder) lies under the NB passing lane, whereas the Girder 1 (the SB exterior girder) lies under the SB slow lane. As such, the Girder 1 is likely to experience more frequent truck traffic than Girder 3. However, at the time when the crack was discovered in Girder 3, the deck surface was being re-laid on this bridge. To facilitate this work, traffic diversions were employed with both NB and SB traffic diverted on to the same structure in single lanes. Thus, Girder 3 might have experienced similar truck traffic as Girder 1 at some period of time.

2.2   Discussion of Instrumentation Plan

The instrumentation plan was developed from experience of conducting field instrumentation programs in steel bridges that have cracked in service. The initial diagnosis was that the Girder 3 had probably developed fatigue cracks due to out-of-plane displacement of the girder web from the rotation of the floor beam. This assessment was made based on the appearance of the crack profile which was concave up or "smiley" and atypical of fatigue cracks induced by out-of-plane distortion. Accordingly, four back to back strain rosettes (CH_1 to CH_12) and eight back to back uniaxial strain gages (CH_13 to CH_20) were provided on the web of Girder G1, local to the termination of the transverse stiffener to web weld near the shelf plate and on both sides of the stiffener. In addition, two LVDTs each were provided on each side of the bearing stiffener (CH_32 to CH_35) normal to the web plate at respectively 2 in and 6 in from the shelf plate (Figure 19) to measure the relative out-of-plane displacement and rotation of the web with respect to the shelf plate.

Another three strain gages were provided at a section on the main girder, two on the flanges and one on the web (CH_21 to CH_23), to determine the through depth strain distribution in the girder near the bearing stiffener and the effect of the bracket shelf plate (Figures 20 and 21).

Two uniaxial strain gages (CH_26 and CH_27) were provided at the inner face of the top and bottom flanges of the Floor Beam FB1 (Figure 22). Similarly, two uniaxial strain gages (CH_24 and CH_25) were provided at the top and bottom flanges of the Cross Girder CG1 (Figures 22 and 23). These gages were provided to determine the moment/rotation of the floor beam and the cross girder.

Two strain gages each were provided in Girders G1 and G3 at top and bottom flanges near the Floor Beam F4 (CH_28 to CH_31). These gages were provided to capture the global response of the bridge under controlled loads.

2.3   Description of Sensors

All uniaxial strain gages were weldable having ¼ in gage length and 350 Ω resistance (Vishay Micro Measurements LWK-06-W250B-350). The strain gage rosettes also had ¼ in gage length and 350 Ω resistance, but were bondable (Vishay Micro Measurements CEA-06-250UR-350). The LVDTs had a range of ± ¼ in.

2.4   Data Acquisition System

Data collection was performed by Campbell Scientific data logger CR9000. Data was collected digitally at rates of 250 Hz and 100 Hz respectively for the controlled load tests and the short term monitoring. To ensure noise-free signals, real time digital filters of 25 Hz and 20 Hz cut-off frequencies were used for the controlled load test and the short term monitoring respectively.

The data logger was enclosed in a weather proof box on the top of the barrier wall at Pier 1 along with the power supply and the communication device.

Remote communication with the logger was established using a wireless modem. Data was downloaded automatically at a preset interval via a server located in the ATLSS Center, Lehigh University. Data were collected and reviewed periodically throughout the monitoring period.

3. CONTROLLED LOAD TEST

3.1 Test Truck

Two PennDOT dump trucks fully loaded and having gross vehicle weight of 59800 lbs and 56800lbs respectively were used for the controlled load tests. The trucks had one front axle and two rear axles. The geometry of the test truck along with the measurement of axle spacing and weights are presented in Tables 1 and 2.

3.2 Description of Tests

Controlled load tests were conducted on November 15, 2006 between 10:00 AM and 11:00 AM using two test trucks of known geometry and weight. Altogether six tests were carried out comprising two crawl tests (essentially static tests) and four dynamic tests to simulate the critical vehicle dispositions. Details of the tests are shown in Table 3. One of the dynamic tests was aborted because the second truck braked in the middle of span and the speed became uncontrolled. For crawl tests, the test trucks were driven across the bridge at approximately 5 mph simulating almost a static loading condition. The dynamic tests were conducted with the test trucks traveling at a normal speed, within the safety limit, typically between 30 to 40 mph. These tests represented the normal in-service condition including the dynamic amplification.

Rolling lane closures were enforced for the load tests. The SB lanes were completely closed for each test and were opened in between successive tests. The test trucks entered the bridge at the North end of Span 4. It was ensured that (i) all others vehicles have exited Span 2 before the test trucks entered the bridge, and (ii) no vehicles entered the bridge before the test trucks crossed Span 2. This measure was necessary both for safety reasons and to ensure that the test results were not confounded by the presence of unknown vehicles.

3.3 Analysis of Test Data

The time history plots of measured data at all channels and for all the controlled load tests are included in APPENDIX A. The collected data was further filtered for plotting and a smoothed time history was generated. Test data from the aborted dynamic test were not plotted. The measured live load strains were converted to stresses by assuming a modulus of elasticity of steel of 29000 ksi. Results from only the crawl test CRWL_2 and the dynamic test DYN_3 are presented here as these test cases were the most severe of all and produced the highest stresses at the strain gages of interest. During crawl test CRWL_2, the trucks traversed side by side across the bridge with the heavier truck on the right lane closest to Girder G1. During the dynamic test DYN_3, the heavier truck crossed the bridge first followed by the other truck, with. both the trucks traveling in the right lane closest to Girder G1.

3.3.1 General Response

Typical plots of stress data from CH_28, CH_29, CH_30 and CH_31 are shown in Figures 24 and 25 for the tests CRWL_2 and DYN_3 respectively. These channels correspond to the uniaxial strain gages located in the span of Girders G1 and G2 While

CH_28 and CH_29 were located respectively on the top and bottom flanges of Girder G1, CH_30 and CH-31 were located respectively on the top and bottom flanges of Girder G3. The strain gages were oriented along the span, with the objective of capturing the primary flexural stresses in the girders. The responses of the girders were typical of moment influence line near the middle of end span of a three span continuous girder. The stresses in the bottom flanges were tensile and that in the top flange were compressive. The compressive stresses were one order of magnitude smaller than the tensile stresses, verifying composite action between the girder flange and the deck concrete. The crawl test demonstrated only one peak in the stress response since the test trucks were traveling side by side, one in each lane. Although Girder G1 has a larger span than the Girder G2 due to the skew at pier P1, and the heavier truck traveled on the right lane closer to G1, the stresses recorded at the bottom flange of Girder G2 was larger probably because the strain gage was located more towards mid span than the one in Girder G1 and because of the disposition of the trucks. The dynamic test demonstrated two stress peaks, each corresponding to the passage of one truck. The first stress peak was higher since the heavier truck crossed the bridge first. The stresses recorded at the strain gages in Girder G1 was larger than that in Girder G2 since the trucks traveled on the right lane, which was closer to Girder G1. In any event, the general response of the girder was consistent with the structural arrangement of the bridge. The maximum recorded live load stress was about 1.5 ksi under the crawl test and that under the dynamic test was about 1.05 ksi. It may be noted that the crawl test discussed here represented a two lane loaded condition, while the dynamic test represented a single lane loaded condition. Comparing to the stresses recorded during crawl test CRWL_1 (Figure 26), which represented a one lane loaded condition (Table 3) with the heavier truck traversing on the right lane, the estimated dynamic amplification in response is about 17%, which is consistent with the recommendations of the current AASHTO bridge design specification.

3.3.2   Local Response near Shelf Plate

Plots of stress data from CH_5 andCH_6 are shown in Figures 27 and 28 for the crawl test CRWL_2 and the dynamic test DYN_3 respectively. These channels correspond to the vertical arms of the strain rosettes provided on both faces of the web at the span side corner of the floor beam connection plate/bearing stiffener to shelf plate junction (Figure 18). The time history plots reflect the disposition of the trucks during the tests and the bridge configuration. The two adjacent/closely spaced stress peaks noted during the crawl test resulted from the two side by side vehicles exiting the bridge at separate times due to the relatively large skew at the South End of the bridge. During the dynamic test the stress peaks were well separated since one truck first crossed the bridge followed by the other. In both loading conditions, however, the stresses on both gages located on the opposite faces of the web plate were in the order of 0.3~0.4 ksi and were compressive. The test data indicated that the live load stresses in the web plate of Girder 1 at location similar to that in Girder 3 was essentially in plane. Out-of plane bending of the web plate due to rotation of the floor beam, as expected earlier, was essentially non-existent.

The live load stresses recorded in the other gages at the same corner (CH_13, CH_14, CH_17, and CH_18) also exhibited similar nature and order of magnitude (Figures 29, 30, 31, and 32).

The principal stresses measured from the strain gage rosette at the outer face of the girder web at the span side corner of the floor beam connection plate/bearing stiffener to shelf plate junction (Figure 18) are plotted in Figures 33 and 35 for the crawl test CRWL_2 and the dynamic test DYN_3 respectively. The directions of the principal stresses with respect to the horizontal arm of the strain gage rosette (sign convention: counter clockwise positive) are shown in Figures 34 and 36. The magnitude of the principal stresses was insignificant. The compressive principal stress was directed towards the corner similar to the bearing end of a simple beam.

Time history of displacements measured at LVDT channels CH_32 and CH_33 are plotted in Figures 37, 38 and 39 for the same two load cases discussed above, which were the most severe among all the controlled load tests. These channels corresponded to the LVDTs located at respectively 6 in and 2 in above the shelf plate on the south side of the floor beam connection plate/bearing stiffener. The test data indicated that maximum out-of-plane deflection of the web plate was 0.14 mils. At the level of top LVDT, the displacement changed sign for both the crawl and dynamic tests as the vehicles exited the span. In fact a relatively large spike in displacement was noted in this LVDT, which suggested of some kind of impact at the expansion joint. At the level of lower LVDT, however, the displacements were always of the same sign. This LVDT was located closest to the cope at the bearing stiffener to the shelf plate junction, where cracking initiated in Girder G3. Nevertheless, the magnitude of out-of-plane displacement recorded by this LVDT was in the order of 0.03 mils, which was insignificant.

3.3.3   Girder G1 near the Connection Plate/Bearing Stiffener

Strain gage channels CH_21, CH_22 and CH_23 were located in a section towards the span side of the floor beam connection plate/bearing stiffener. The channels CH_21 and CH_23 were located on the inner face of the top and bottom flanges respectively, whereas the CH_22 was located on the web (Figure 18). The time histories of measured stresses at these gages are shown in Figures 40 and 41 for the crawl test CRWL_2 and dynamic test DYN_3. The stress distribution through the depth of the Girder G1 at this section is affected by the presence of the bearing shelf supporting the simple Span 1. The reaction from Span 1 generates tensile stress in the bearing shelf and compressive stress in the bottom flange of the bracket projection. The compressive stress in the bottom flange of the bracket develops into Span 2 beyond the bearing center line, producing compressive stress in the bottom flange of the Girder G1 at this section. Because of the proximity of this section to the bearing center line, the reaction from Span 2 generates only small tensile stress in the bottom flange, which is insufficient to surpass the compressive stress. The stress measured at the web gage CH_22 is tensile, as the contributions from the top flange of the bracket/bearing shelf plate and Span 2 are both additive. The stresses measured in the top flange of Girder G1 (CH_21) are relatively small due to the composite action between the girder and the concrete deck. The maximum measured tensile stress at this section was about 0.35 ksi.

3.3.4   Cross Girder CG1

Time history plots of stresses measured at channels CH_24 and CH_25, located in Cross Girder CG1 (Figure 18), are presented in Figures 42 and 44 for the crawl test

CRWL_2 and the dynamic test DYN_3. Reversal of stresses was noted as the test trucks entered Span 1 from Span 2. This response is possible since the Cross Girder CG1 ties the ends of the bracket projections from Girders G1 and G2. When the test trucks are on Span 2, the Girders G1 and G2 undergo sagging deformation causing the bracket projection to move upwards. As a result, compressive and tensile stresses develop respectively in the top and bottom flanges of the cross girder. However, when the test trucks are on Span 1, the bracket projections displace downwards. To be compatible with this deformation, the cross girder bows up near the connection with the girders, generating tensile and compressive stresses in the top and bottom flanges respectively. The effect of this deformation was small however, and the maximum stresses recorded during the load tests were about 0.3 ksi.

3.3.5   Floor Beam FB1

Stresses measured at the gages located on the inner faces of the top and bottom flanges of the Floor Beam FB1 (CH_26 and CH_27) are plotted in Figures 44 and 45 for the crawl test CRWL_2 and dynamic test DYN_3 respectively. Because of the composite action with the concrete deck, the top flange stresses were generally lower than the bottom flange stresses by an order of magnitude. During the dynamic test, however, the compressive stress in the top flange was almost as large as the tensile stress in the bottom flange when the test trucks crossed the expansion joint between the Spans 1 and 2. The tensile stresses in the bottom flange went through reversal under both the crawl and the dynamic tests as the test trucks crossed over the expansion joint. This behavior was probably due to the dynamic impact generated from the trucks crossing over the uneven expansion joint. The maximum measured stress in the floor beam was about 0.3 ksi.

3.4   Discussion

The controlled load tests exhibited small live load stresses in the Girder G1 at the locations corresponding to cracked web in Girder G3. No significant evidence of out-of-plane bending of the girder web under live load stresses was found and the magnitude of the stresses was too low to suggest any such activity. As such, it was concluded that the web cracking in Girder 3 was probably not due to fatigue induced by out-of-plane bending of the web plate. Further discussion on the findings is provided in Section 8.

4. SHORT TERM MONITORING

The strains and displacements at the installed sensors were monitored for a period of 30 days between 11/14/06 and 12/13/06 under in-service traffic.

4.1 Monitoring Strategy

During short term monitoring stress time-history data were not collected continuously. Data were only recorded when the measured stress at the span bottom flange gages (CH_29 and CH_31) exceeded a predefined trigger of 1.35 ksi. This trigger value was set after monitoring the stresses at these gages for about a day under normal in-service traffic. Too low a threshold would have recorded a large amount of data corresponding to usual in-service live load stress events that were too small to cause any fatigue damage or fracture and as such were of little interest. Once the strain value for the "trigger" gage reached the preset limit, the logger recorded data at all channels for a predefined period of approximately 23 seconds, consisting of 15 seconds of pre-trigger data. The triggered data provided record of stresses at the monitored locations in girder G1 that were generated from the passage of heavier vehicles. The girder G3 also probably experienced similar stress histories, and the records provided a basis for examining whether these stress events could have initiated cracking in the girder G3.

4.2 Analysis of Live Load Stresses

Stress-range histograms were developed for each of the monitored strain channels using the *rainflow* cycle-counting algorithm available with the data logger. For each channel, time-history data were analyzed every 10 minutes and the peaks and valleys in the response were paired to determine a tally of stress ranges. Twenty bins were defined within a minimum and maximum stress range limits of 0 and 10 ksi respectively, resulting in a bin size of 0.5 ksi. The first bin containing stress ranges less than 0.5 ksi was ignored, since contribution to this bin is mostly due to spurious noise signals.

4.3 Stress Range Histograms

Histograms of live load stress ranges measured at the strain gage rosettes on the span side web of Girder 1 (channels CH_1 to CH_6) near the possible crack origin are shown in Figures 46 and 47.

Stress range histograms obtained at other strain channels were insignificant except for the channels CH_29 and CH_31, which were located at the tension flanges of Girders G1 and G2 respectively.

4.4 Discussion

The live load stress ranges near the bracket shelf plate were less than 1.5 ksi under both controlled loads and in-service traffic. Noting that the fatigue threshold for the most severe AASHTO detail category E′ is 2.6 ksi, fatigue crack propagation in the girder web under usual traffic condition is unlikely.

5. FORENSIC INVESTIGATION

Holes were drilled at the crack tips in the web of Girder G3 to arrest possible crack growth. One of the cores retrieved from these holes contained part of the crack surface. The fracture surface and the crack front was exposed by brittle fracture after cooling down the core to cryogenic temperature.

5.1 Visual Inspection

The exposed fracture surface is shown in Figure 48. The crack surface was substantially corroded, which indicated that it was probably a few years old. No evidence of paint marks was noted on the crack surface, however.

5.2 Fractographic Examination

Examination of the crack surface under scanning electron microscope (Figures 49 and 50) revealed cleavage facets indicating that the cracking of the web had occurred by cleavage fracture rather than stable fatigue crack growth.

5.3 Additional Studies

Subsequently, efforts were made to core out the web of Girder 3 as close to the bearing stiffener to the shelf plate intersection as possible with the purpose of determining the crack origin. This effort was unsuccessful by the presence of floor beam connection plate and bearing stiffener on the inside face of the girder web, which prevented the core drilling bit from penetrating through (Figure 51). Further investigation on the source of cracking was continued with material testing of the girder web.

6.   MATERIAL TESTS

In order to find out the reason for brittle fracture, material tests were conducted on the material of the web of Girder 3.

The properties of the girder web material were examined further to investigate the occurrence of cleavage fracture of Girder 3. Approximately 4.5 in × 7 in piece was cut out from the edge of the fractured web adjacent to the cracked surface. Schematic of cutting plan are shown in Figure 52. Twelve Charpy V-Notch (CVN) specimens and two tensile specimens were carved out from this cut-piece as shown in Figure 53. Chemical composition of the web steel was also determined.

6.1   Evaluation of Strength

Two standard 505 tensile specimens were prepared. The tensile tests were conducted at the 600 kip SATEC universal testing machine in the ATLSS Center, Lehigh University. The tests were conducted at a loading rate of 1.6×10^{-3} in/in/s, which corresponded to a static (slow) loading rate and conformed to ASTM A370.

Stress-strain plots of the web steel from the tensile test are presented in Figures 54 and 55. The material demonstrated a yield and tensile strength of respectively, about 40 and 70 ksi. The stress-strain curves are typical of A36 steel, showing upper and lower yield points, yield plateau, and strain hardening.

6.2   Evaluation of Toughness

Twelve CVN specimens were prepared, having section width equal to the available thickness of the girder web of about 3/8 in (≈9.5 mm), which was less than the standard size of 10mm. In the depth direction the section size was maintained at the standard size of 10 mm. Since the thickness of the girder web was close to the standard size of a CVN specimen, the same thickness was maintained to obtain a more accurate assessment of fracture toughness of the girder web. If the fracture toughness is corrected for a standard 10 mm thickness, the measured value is to be increased in the ratio of the section widths, i.e., by about 5%. This correction was ignored to obtain a more conservative assessment.

Notch in nine of the CVN specimens were oriented such to provide toughness in the longitudinal direction (rolling direction or L-T orientation). Three other CVN specimens were prepared to determine the toughness in the transverse direction (T-L orientation). The CVN tests were conducted at four discrete temperatures of 0^0, 40^0, 80^0, and 120^0 F. At three of these temperatures each, two specimens were tested for toughness in the longitudinal direction and one specimen was tested for toughness in transverse direction. At 120^0 F all three specimens were tested for toughness in the longitudinal direction.

The CVN test results are shown in Figures 56 and 57. The results exhibited a toughness of the web steel of about 30 ft-lb at 40^0 F in the longitudinal direction, which is more than the required 25 ft-lb at 40^0 F for Fracture-Critical Members in Zone 2, as per the current AASHTO Bridge Design Specification. In the transverse direction, however,

the toughness at 40^0 F was about 13 ft-lb, which was substantially less than the minimum toughness of 20 ft-lb.

6.3   Chemical Analysis

Chemical analysis of the web plate is presented in Appendix 1. The testing was conducted by Laboratory Testing Inc, Hatfield, PA. The analysis result indicates that the steel conforms to ASTM A36 as indicated in the construction drawings.

6.4   Discussion of material test results

This low toughness in the transverse direction explains the observed cleavage fracture surface in the web of Girder G3. Differences in mechanical properties of hot rolled steel plates measured along the rolling direction (L-T orientation) and transverse to this direction (T-L orientation) are commonly observed, particularly in plates manufactured in the past. This difference is primarily due to the effects of hot rolling on the resulting shape of non-metallic inclusions in the steel. Hot rolling tends to flatten and elongate inclusions along the rolling direction which can vary the tensile strength, tensile ductility, and notch toughness of the steel measured in the two directions. This difference is markedly reduced in modern day steel plate by (a) cross rolling which subjects the plate to the effects of rolling in multiple directions and (b) reductions in the concentration of non-metallic inclusions.

7. FINITE ELEMENT ANALYSES

A limited linear elastic Finite Element Analysis (FEA) was conducted to verify the stresses obtained from the field measurements. A detailed three dimensional (3-D) model of the bridge superstructure was prepared in ABAQUS, a commercially available FEA code. The model was analyzed for four load cases representing four instantaneous positions of the trucks during the controlled load tests. The FEA results were compared with the controlled load test results.

7.1 The Finite Element (FE) Model

7.1.1 The Model Configuration

A detailed 3-D model of the continuous bridge superstructure module comprising Spans 2, 3 and 4 between Pier 1 and North Abutment was developed (Figure 58). The model consisted of all components of the superstructure including the deck, the main girders, the floor beams, the stingers, the cross girder. The bearing stiffeners, the floor beam and cross girder connection plates, the floor beam seats at connection plates and the intermediate transverse stiffeners at the floor beam connections were included in the girder models. All transverse stiffeners in the cross girders and floor beams were also included (Figures 59 and 60). However, the other transverse intermediate stiffeners and the longitudinal stiffeners in the girders, and the transverse wind bracings between the girders were excluded from the model, as these elements have little effect on the global structural response under vehicular live load. These exclusions are also unlikely to affect the stress field local to the web gap at the transverse bearing stiffener near the termination of the bearing stiffener/floor beam connection plate-to-web weld above the bracket shelf plate, which is the region of interest as the possible origin of web cracking similar to Girder G3. Similar other exclusions were the stiffeners in the stringers and the diaphragms.

Both the parapet and the kerb were included in the deck, as these elements affect the structural response of a bridge significantly, where the deck is composite with the girders. The model also included the haunches between the girder compression flanges and the deck. All variations in width and thickness of the girder flanges were incorporated in the model. In certain areas, however, minor local variations were introduced in the model for the sake of simplicity, without compromising the global response characteristics. None of the bolted and welded connections were modeled, and the copes in the transverse members were not included. All welded connections were considered monolithic, and the bolted connections were considered constrained. The interactions between the various elements and components of the superstructure were suitably constrained.

One important aspect of the FE model relevant to the local stress field at the web gap in the transverse bearing stiffener/floor beam connection plate above the bracket shelf plate at Pier 1 was the modeling of the bearing stiffener/connection plate to the bracket shelf plate junction. The full depth bearing stiffeners at Pier 1 are interrupted by the bracket shelf plate in the girders. The bearing stiffeners at this interface are mill finished for tight fit with no weld. The floor beam connection plates are also interrupted by the bearing shelf plate, however, a gap of 1 in is provided in the connection plate

above the bearing shelf. Below the bearing shelf the connection plate is mill finished and tight fitted to the shelf plate with no weld. A cope of about 1 in × 1 in is provided in the fitted stiffeners/connection plates for uninterrupted passage of the welds between the shelf plate and the girder web. To simplify the interface modeling, the fitted bearing stiffeners and connection plates were terminated 1 in short of the shelf plate surfaces. Although this simplification will interrupt the load transfer path in the bearing stiffeners by direct contact, and may influence the local in-plane stress field by creating deviator stresses, the effect should be of little concern since the bearing stiffeners are essentially under compression. Considering the susceptibility of the web gaps to distortion induced secondary out-of-plane stresses of relatively large magnitude, where the stiffeners are not positively attached to the flanges, this simplification is all the more justified because of the 1 in × 1 in copes in the stiffeners, which create the web gap condition. Large out of plane bending stresses may develop in the web gaps initiating fatigue cracks from initial discontinuities in the shelf plate to girder web welds. Thus, this idealization is reasonable for capturing any distortion in the web gap and for identifying the source of cracking in the girder webs.

7.1.2 Material Properties

All elements of the superstructure are of structural steel except for the concrete deck. All material models were considered as linear elastic. The modulus of elasticity and Poisson's ratio of steel were assumed respectively as 29000 ksi and 0.3. These parameters for the deck concrete were considered as 2900 ksi and 0.15 respectively.

7.1.3 Boundary Conditions

Displacement boundary conditions consistent with fixed and expansion bearings were applied to the underside of the girder flanges at the bearing stiffener locations. The bearing at Pier 2 is fixed and the others are of expansion type.

7.1.4 Loading

The model was analyzed for four load cases representing four instantaneous positions of the trucks during the controlled load tests:

Load Case 1 – Truck positions corresponding to the maximum values at the strain gage channels CH_29 and CH_31 respectively, in the spans of Girders G1 and G2 during the crawl load test CRWL_2 (Table 3). The estimated wheel positions are shown in Figure 61.

Load Case 2 – Truck positions corresponding to the maximum values at the strain gage channel CH_31 in the span of Girder G2 during crawl load test CRWL_1 (Table 3), when the truck 797-8076 was traversing the left lane. The estimated wheel positions are shown in Figure 62.

Load Case 3 – Truck positions corresponding to the maximum values at the strain gage channel CH_29 in the span of Girder G1 during crawl load test CRWL_1 (Table 3), when the truck 531-8076 was traversing the right lane. The estimated wheel positions are shown in Figure 63.

Load Case 4 – Truck positions corresponding to the maximum values at the strain gage channels CH_5 and CH_6 near the web gap at the bearing stiffener/floor beam connection plate above the bracket shelf plate in Girder G1 at Pier 1 during crawl load test CRWL_1 (Table 3), when the truck 531-8076 was traversing the right lane. The estimated wheel positions are shown in Figure 64.

7.1.5 Elements

Twenty node quadratic reduced integration isoparametric 3D continuum elements were used for analyses. The entire model consisted of 755,277 elements and 4,029,971 nodes with 12,089,913 solution variables or nodal degrees of freedom.

7.2   FEA Results

The relevant FEA results of Girders G1 and G2 are shown in Figures 65 to 73 for the analyzed load cases. Figure 65 shows the contour of longitudinal or normal stress in the Girders G1 and G2 under Load Case 1 corresponding to controlled load test CRWL_2. The stress contour is typical of the flexural response of a beam under in plane transverse loading. The neutral axis is located high up in the web near the deck soffit owing to the composite action with the deck. The stress in G2 is higher than that in G1, because of the lane disposition and the resulting placement of wheel loads closer to G2.

Figures 66 to 71 show the relevant part profiles of longitudinal stress at the inner face of bottom flanges of the Girders G1 and G2 along the indicated paths for the Load Cases 1, 2 and 3. The discontinuities in the stress profiles correspond to the location of floor beams, where the seats under the floor beams are connected to the bottom flange. Also plotted on these figures are the point measurements of stresses at the strain gage channels CH_29 and CH_31 as appropriate. It is evident that the FEA results consistently over predicted the stresses in the girder flanges. While the estimated stresses in Girder G1 were higher than the measured values by about 10~20%, the estimated stresses in Girder G2 were about 60~62% higher. This is not surprising, since the analysis results are known to always over predict the actual field measurements due to various reasons including, simplified assumptions in the analysis models and boundary conditions, the nonlinearities in the responses owing to complex contact interactions and load transfer among the members and component, etc. The estimated and measured stresses, nevertheless, were of the same order of magnitude.

Figures 72 and 73 show the principal stress fields near the web gap in the bearing stiffener/floor beam connection plate respectively on the outer and inner faces of Girder G1 at Pier 1 under Load Case 4. The maximum and minimum principal stresses measured on strain rosette channels CH_1, CH_3 and CH_5 are respectively 0.32 ksi and -0.58 ksi. The estimated and measured stresses are of the same order of magnitude.

7.3   Discussion

The FEA results provided good agreement with the measured stresses, particularly in the Girder G1. The analysis verified the relatively low stresses measured during field monitoring, specifically local to the web gap above the bracket shelf plate, which is the region of interest as the possible origin of web cracking similar to Girder G3.

8.   ASSESSMENT, RECOMMENDATIONS AND CONCLUSION

8.1   Assessment

Based on the field instrumentation, controlled load test, short term monitoring, fractographic investigation material tests and finite element analyses, it appears that cracking of the web of Girder 3 was due to cleavage fracture that probably initiated from a flaw condition at the termination of the transverse stiffener to web weld near the cope, during an unusually extreme load event, such as low temperature and/or impact from overloading. The flaw condition could be due to a relatively large weld fabrication defect or propagation of fatigue crack from micro discontinuities. Efforts were made to core out any such flaw at the crack origin for examination, but in vain. Due to the presence of floor beam and bearing stiffeners close to each other near the crack origin, the core could only be drilled away from the origin. Limited FEA verified the relatively small live load stresses measured at the web gap, which was insufficient to cause fatigue crack propagation under service loading.

The dynamic impact from an overload is suspected because of the proximity of the crack to a deck expansion joint, which are known to introduce irregularity in riding surface and cause impact loading. The replacement of deck joint in June 2006 and the deck in the fall of 2006 suggest that the riding surface was sufficiently deteriorated to create such a condition. In addition, this route being located around Philadelphia, experiences heavy truck traffic, many of which are often permit loads and undetected overloads.

Another reason for this cracking could be the over-constraint provided by the floor beam connection plate, the bearing stiffeners and shelf plate, all of which are welded to the web in close proximity near the crack location. As such, the web plate is under high tensile residual stress field at this junction. The existing copes in the connection plates/stiffeners are too small to provide sufficient relief to the constrained condition. On the contrary, presence of small gaps in this highly constrained region may create a crack like condition that can initiate unstable fracture.

8.2   Recommendations

To prevent cracking at similar locations in other girders, it was recommended to drill 2 in diameter holes on either side of the floor beam connection plate/bearing stiffener and just above the longitudinal weld between the bracket shelf plate and the web of the girders. The holes were drilled as close to the stiffeners as possible. The edges of the holes were ground smooth to remove any possible stress concentration from surface irregularities that might become initiators of fatigue cracks. In case of any unstable crack growth these holes are expected to act as crack arrestors. These holes are also expected to provide some relief to the constraint condition that may exist at the intersection of bearing shelf plate, floor beam connection plate and bearing stiffeners. The girder ends should also be inspected at the existing inspection cycle of two years interval.

8.3   Conclusion

Based on the limited field monitoring data and controlled load test results near the bracket shelf plate in Girder 1, FEA results, and the forensic studies of the crack location in Girder 3, there should not be any concern for fatigue cracking leading to unstable fracture in the girders of Span 2 near the Pier 1, after the preventive holes are drilled. The live load stresses measured in Girder 1, near the geometrically similar cracked corner of Girder 3, was less than 1.5 ksi, which is unlikely to promote fatigue crack propagation. The fracture toughness of the web steel is about 30 ft-lb at 40^0 F in the longitudinal direction, which is more than the required 25 ft-lb at 40^0 F for Fracture-Critical Members in Zone 2, as per the current AASHTO Bridge Design Specification. The cracking in Girder 3 was an unusual event, which was probably initiated by the combination of an extreme event/constraint and the low material fracture toughness in the transverse direction (in the depth direction) of the web (about 13 ft-lb at 40^0 F). Any possible unstable cracking in the girder webs, from the junction of floor beam connection plate, bearing stiffener and the shelf plate, should be arrested by the holes drilled on either side of the connection.

TABLES

Table 1 Geometry of Test Truck

Truck No.	Rear Axle	L1 (in)	L2 (in)	W_f (in)	W_r (in0	A (in)	B (in)	C (in)	D (in)	E (in)
797-8076	Tandem	163	50	87	72	*	13	22	*	9
531-8076	Tandem	163	50	*	*	*	*	*	*	*

* Dimension not measured
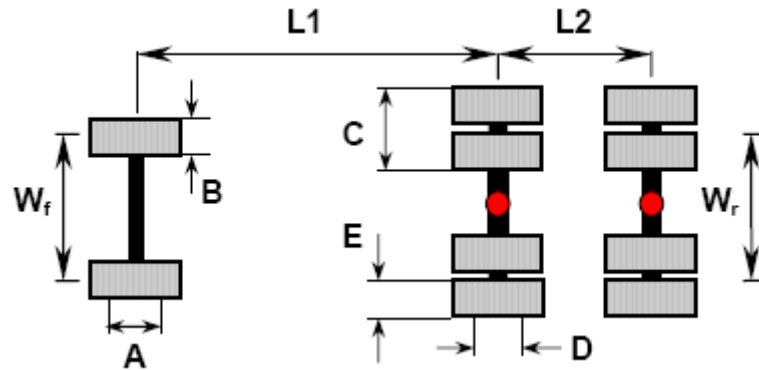
Table 2 Weight of Test Truck

Truck No.	Wheel	Weight of Axle (lbs)			
		1st	2nd	3rd	Total
797-8076	Right	7650	9600	9100	26350
	Left	7750	11200	11500	30450
	Total	15400	20800	20600	56800
531-8076	Right	7400	10850	10500	28750
	Left	7700	11650	11700	31050
	Total	15100	22500	22200	59800

Table 3   Details of Controlled Load Test

Test No.	Test ID	Start Time	Left Lane		Right Lane		Notes
			Truck No.	Speed (mph)	Truck No.	Speed (mph)	
1.	CRWL_1	9:59 AM	797-8076	5	531-8076	5	1
2.	DYN_1	10:14 AM	797-8076	40	531-8076	35	1,2
3.	DYN_2	10:22 AM	531-8076	38	–	–	1
			797-8076	40	–	–	
4.	DYN_3	10:36 AM	–	–	531-8076	40	1
			–	–	797-8076	45	
5.	CRWL_2	10:47 AM	531-8076	5	797-8076	5	3
6.	DYN_4	11:00 AM	797-8076	30	531-8076	40	4

[1] Truck 531-8076 crossed the bridge first, followed by Truck 797-8076

[2] Truck 797-8076 followed Truck 531-8076 closely and braked in the middle of span; test aborted

[3] Trucks were side by side

[4] Repeat of Test 2, but Truck 797-8076 crossed first followed by Truck 531-8076

FIGURES
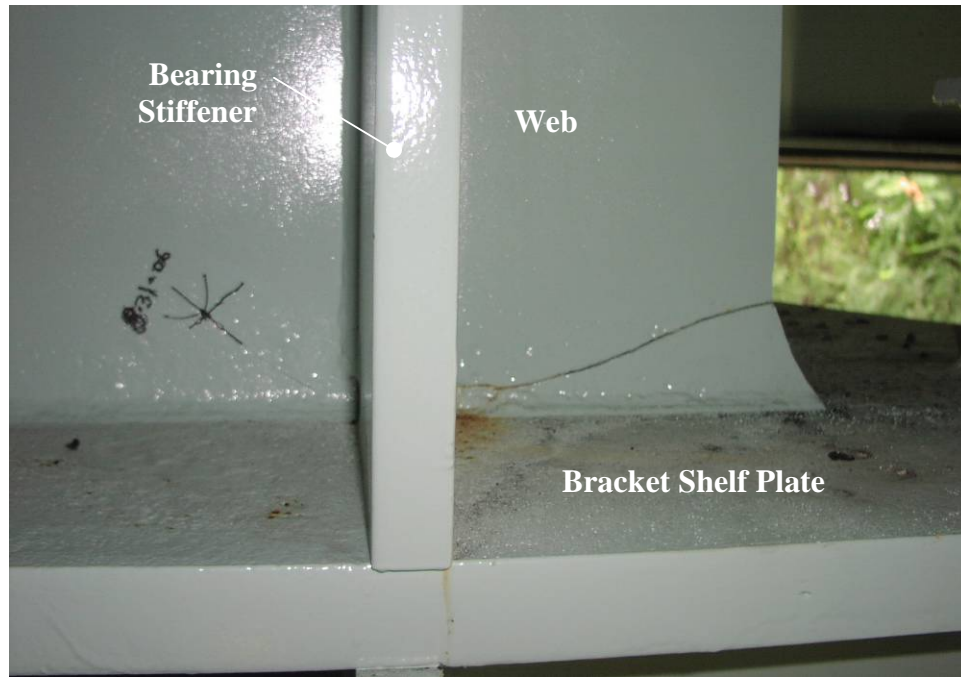
Figure 1   **Crack detected in the web of Girder 3**

Figure 2   **Elevation of bridge — Span 1 and Span 2**

Figure 3   Elevation of bridge — Span 2 and Span 3
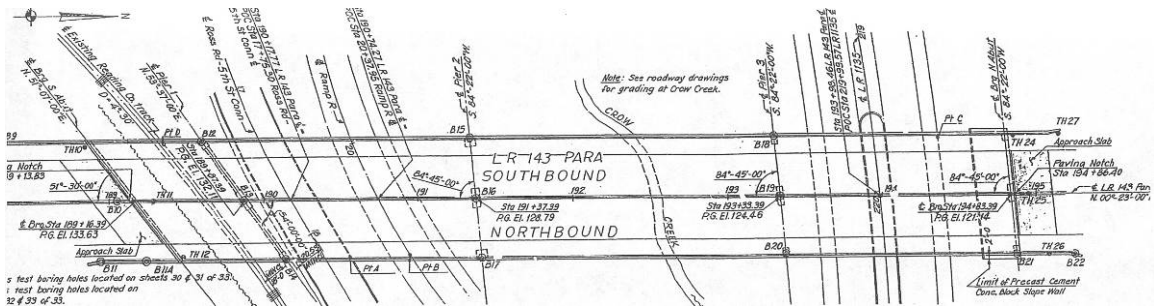
Figure 4   Plan of Bridge SR 46-3020
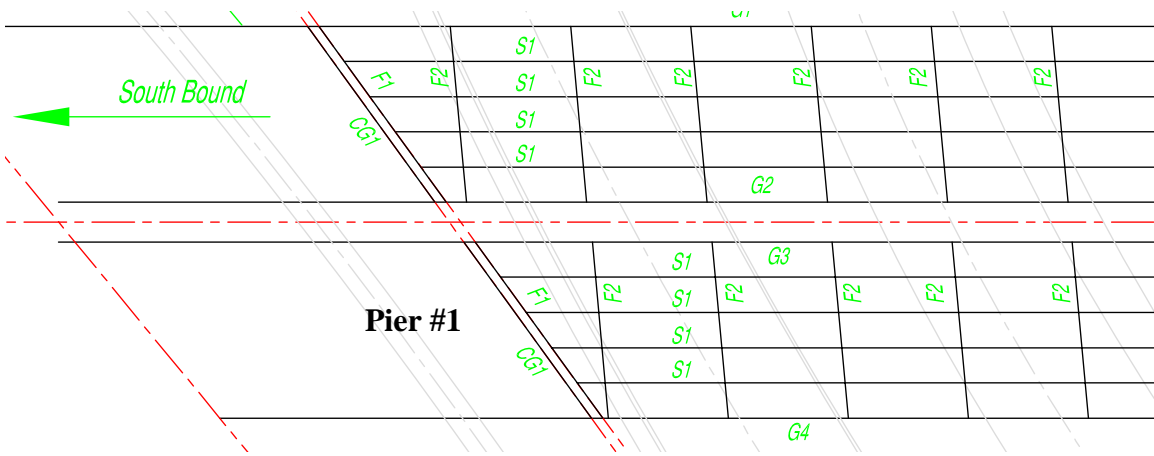
Figure 5   Top framing plan of Span 2

Figure 6   **Deck framing plan at Pier 1**

Figure 7   **At Pier 1 girders connected by floor beam and cross girder parallel to the skew.**

Figure 8 **At Pier 1 cross girder connecting bracket projection from the main girders of Span 2.**

Figure 9 **Bearing stiffener at bracket shelf plate**

Figure 10 **Bracket shelf plate at floor beam connection plate**

Figure 11 **Seating of Span 1 on bracket projection from girder of Span 2**

Figure 12   Crack origin (north side of bearing stiffener)

Figure 13   Crack origin (south side of bearing stiffener)

Figure 14   Holes drilled at crack tips

Figure 15   Access to underside of bridge deck

Framing Plan

CH_28 Top Flg
CH_29 Bot Flg

CH_30 Top Flg
CH_31 Bot Flg

5'

Q of Existing Railway Track

Detail A

South Bound

N

G1

S1
S2
S3
S4

G2

S1
S2
S3
S4

G3

G4

F1 F2 F3 F4 F5 F6 F7 F8 F9

CG1

F1 F2 F3 F4 F5 F6 F7 F8

CG1

DETAIL A

Girder 1

A
B

C

Floorbeam 1

Cross Girder 1

C

A
B

NO. DESCRIPTION   DATE   BY

DESIGNED BY: SR/BTY
DRAWN BY: JDK
CHECKED BY: SR
SCALE: 1/2" = 12'-0"
DATE: 10/30/06
PROJECT NO.:   PROJECT NO.
SHEET TITLE:

SPAN 1
FRAMING PLAN

SHEET NO.:

1 OF 3

Figure 16   Instrumentation Plan (Sheet 1 of 3)

CH_26

2'-6"

CH_27

Section A-A
(FLOORBEAM 1)
LOOKING SOUTH

NOTE: Gages are installed 3" from the edge of the flange.

2 LVDTs
CH_34 Top
CH_35 Bot

GIRDER 1

2 LVDTs
CH_32 Top
CH_33 Bot

D

D

Floorbeam 1

Cross Girder 1

Section D-D
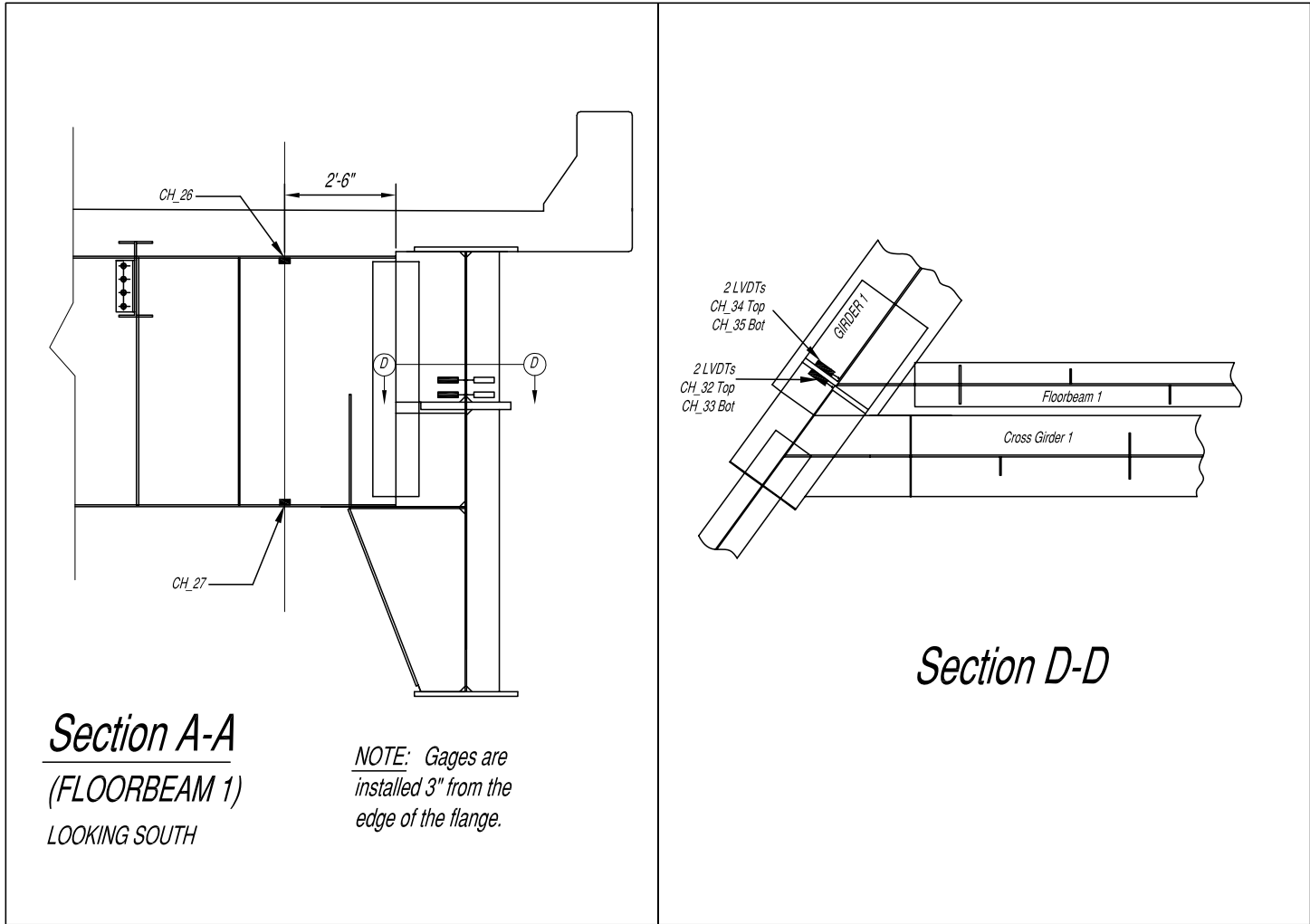
ATLSS

ADVANCED TECHNOLOGY FOR
LARGE STRUCTURAL SYSTEMS
117 ATLSS Drive
Lehigh University
Bethlehem, PA 18015
610-758-3535   FAX 610-758-6842

PROJECT:

BRIDGE SR3020
ON US202
(MARKLEY ST)

SHEET NOTES:

NO. DESCRIPTION | DATE | BY

DESIGNED BY: SR/BTY
DRAWN BY: JDK
CHECKED BY: SR
SCALE: 1/2" = 1'-0"
DATE: 10/30/06
PROJECT NO.: PROJECT NO.
SHEET TITLE:

PLAN VIEW OF
GIRDER G1 NEAR
PIER 1
SHEET NO.:

2 OF 3

Figure 17   Instrumentation Plan (Sheet 2 of 3)

31

Section B-B
(Cross Girder 1)
LOOKING SOUTH

CH_24

2'

CH_25

NOTE: Gages are installed 3" from the edge of the flange.

Section C-C
Girder 1
Looking East

1'

CH_19 N.S.
CH_20 F.S.

CH_15 N.S.
CH_16 F.S.

CH_21

CH_17 N.S.
CH_18 F.S.

CH_13 N.S.
CH_14 F.S.

X Axis CH_1 N.S. CH_2 F.S.
Z Axis CH_3 N.S. CH_4 F.S.
Y Axis CH_5 N.S. CH_6 F.S.

X Axis CH_7 N.S. CH_8 F.S.
Z Axis CH_9 N.S. CH_10 F.S.
Y Axis CH_11 N.S. CH_12 F.S.

CH_22

3"

Web of CG1

CH_23

NOTE: CH_21 & CH_23 are installed 3" from the edge of the flange.

Figure 18   Instrumentation Plan (Sheet 3 of 3)

Figure 19   **Arrangement of LVDTs on the span side of bearing stiffener**

Figure 20   **Location of strain gage channel CH_22**

Figure 21   Location of strain gage channel CH_23
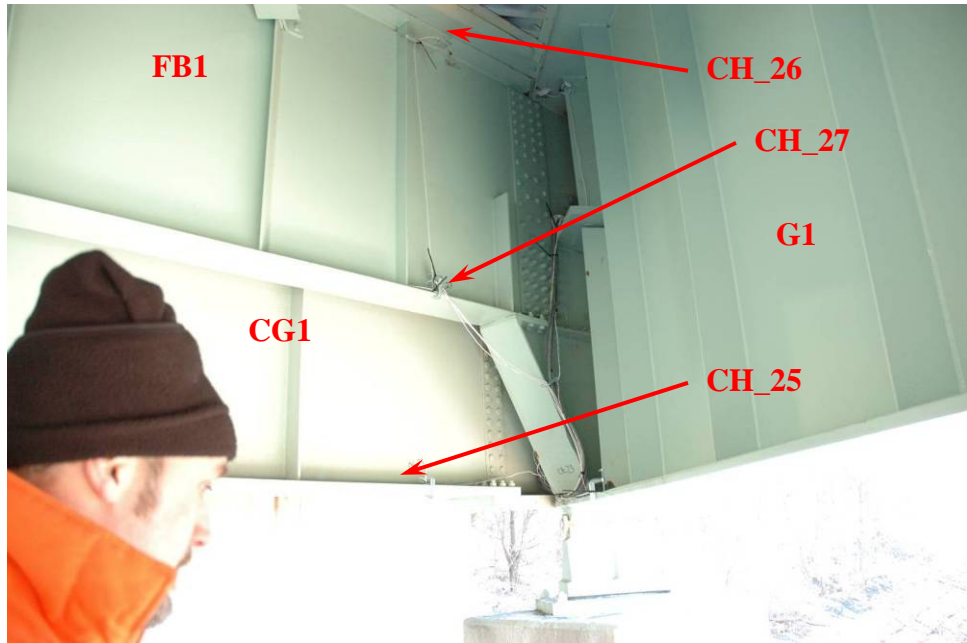
Figure 22   Locations of strain gage channels CH_25, CH_26 and CH_27
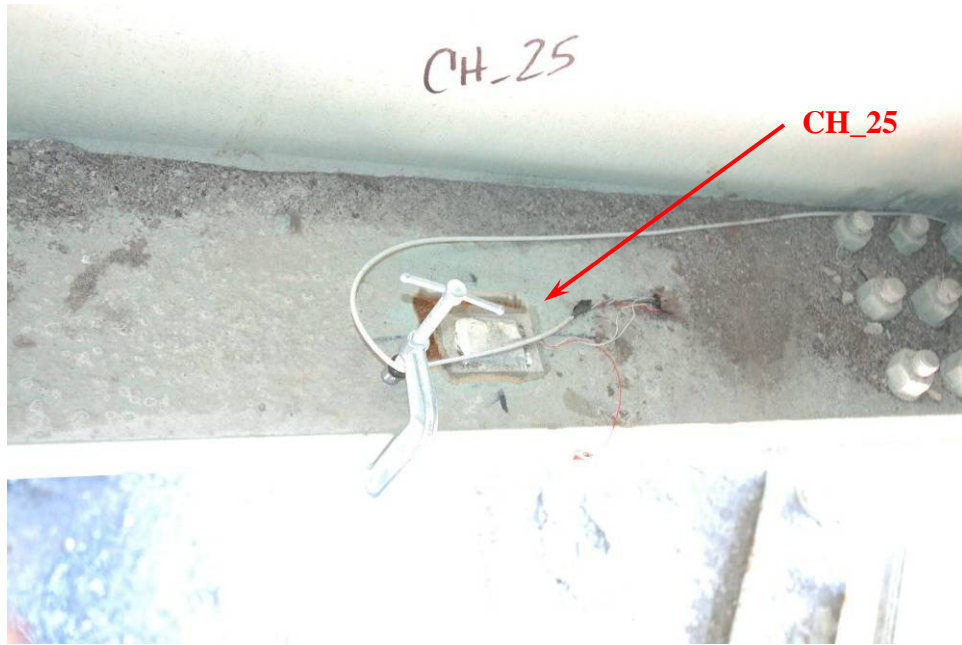
Figure 23   Strain gage channel CH_25
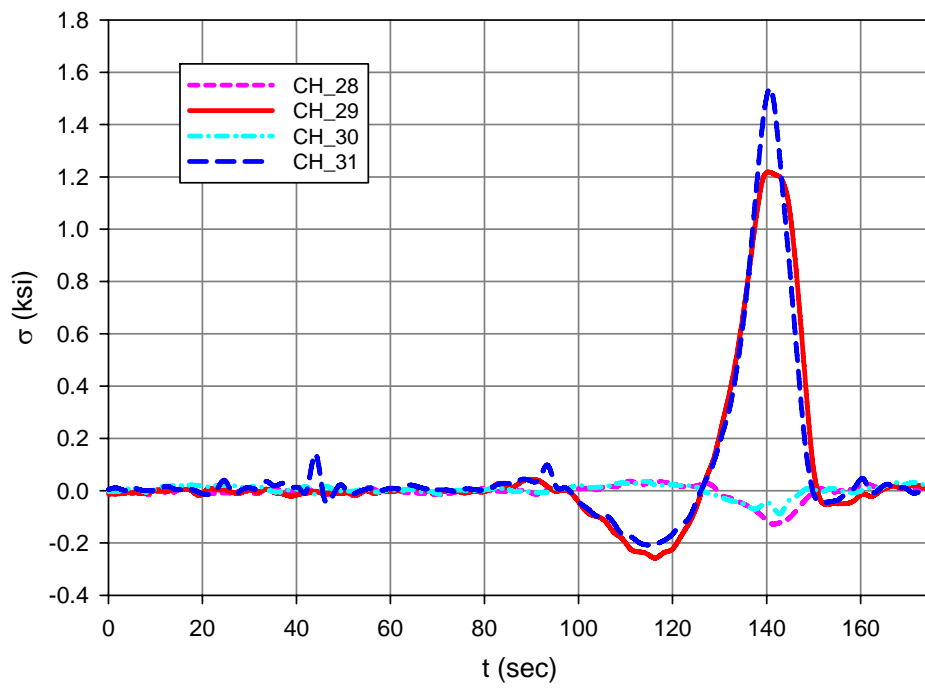
**Figure 24   Stresses measured at the span gages during crawl load
             test CRWL_2**
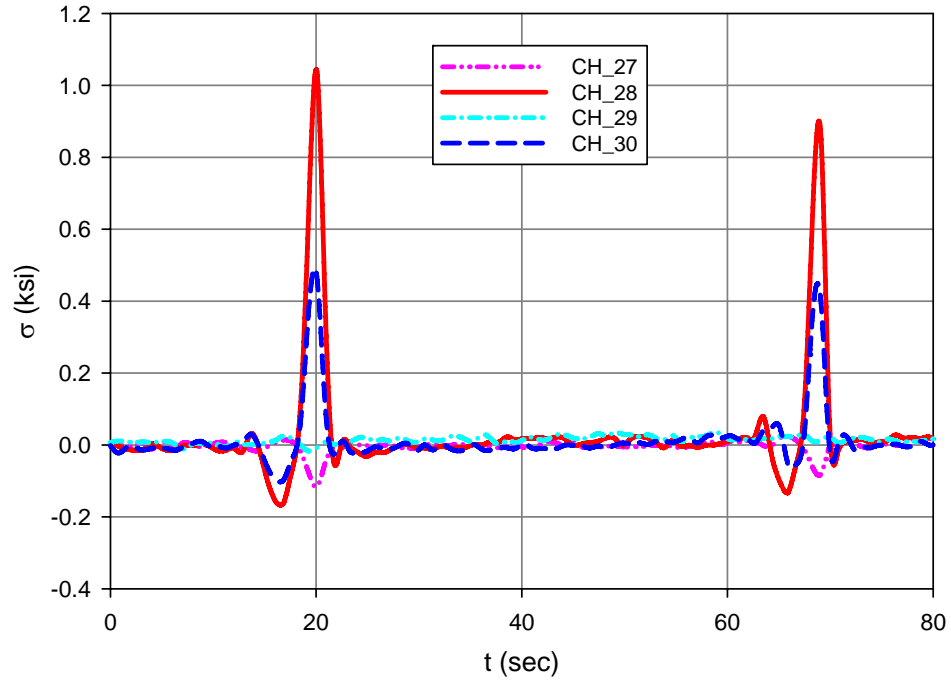
Figure 25   **Stresses measured at the span strain gages during dynamic load test DYN_3**
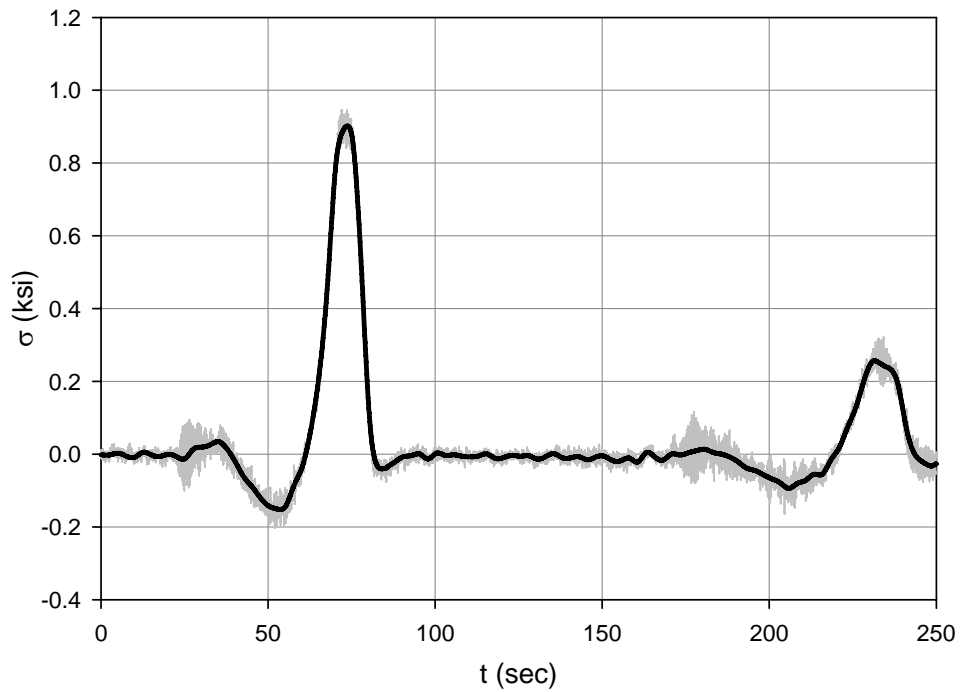
Figure 26   **Stress measured at span bottom flange strain gage CH_29 in Girder G1 during crawl load test CRWL_1**
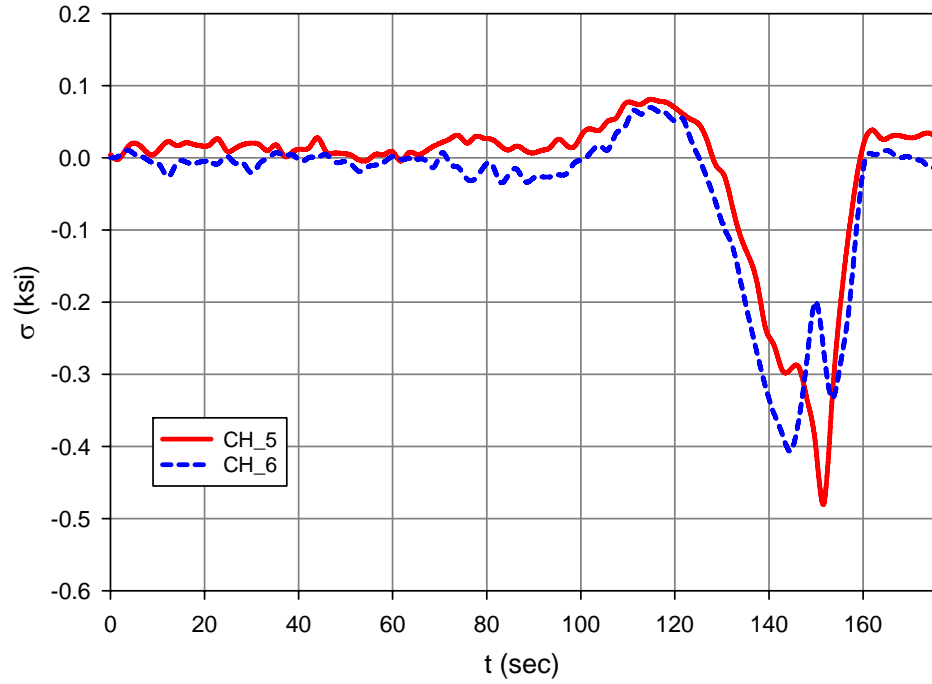
Figure 27 **Stresses measured at strain gage channels CH_5 and CH_6 during crawl load test CRWL_2**
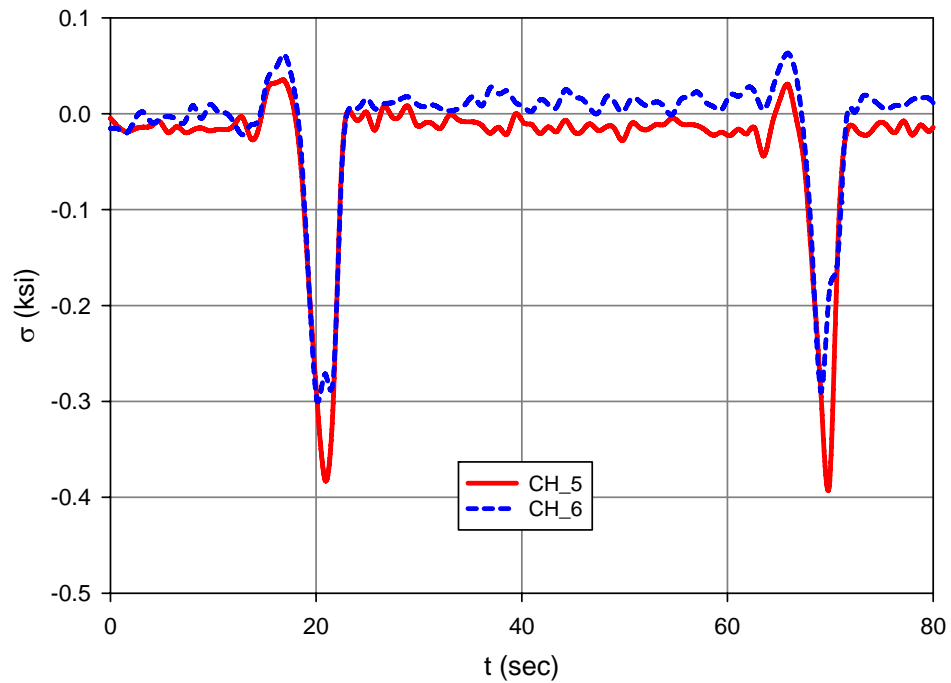
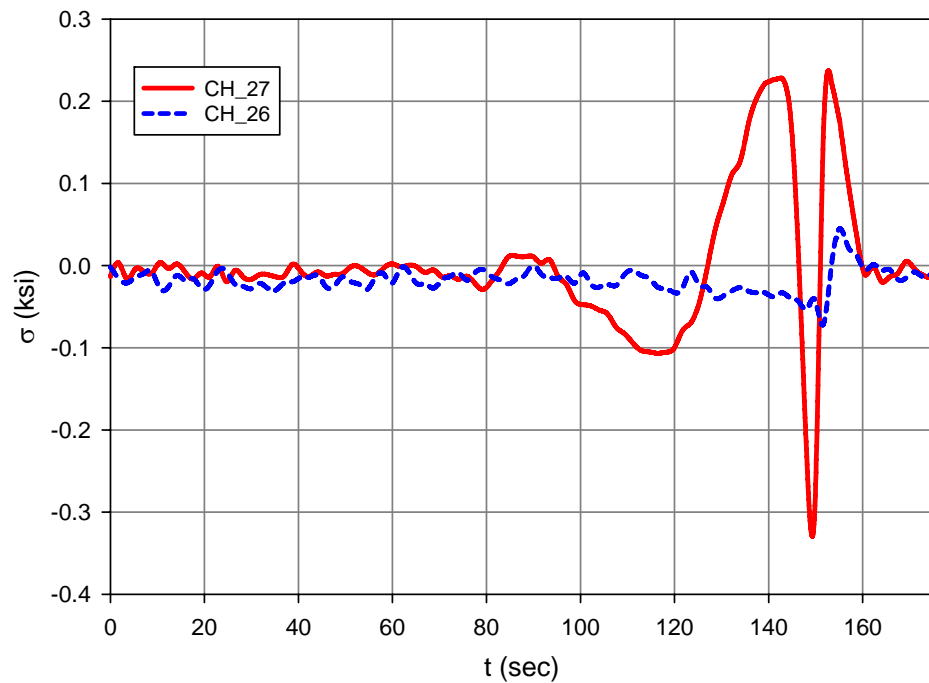**Figure 28** **Stresses measured at strain gage channels CH_5 and CH_6 during dynamic load test DYN_3**
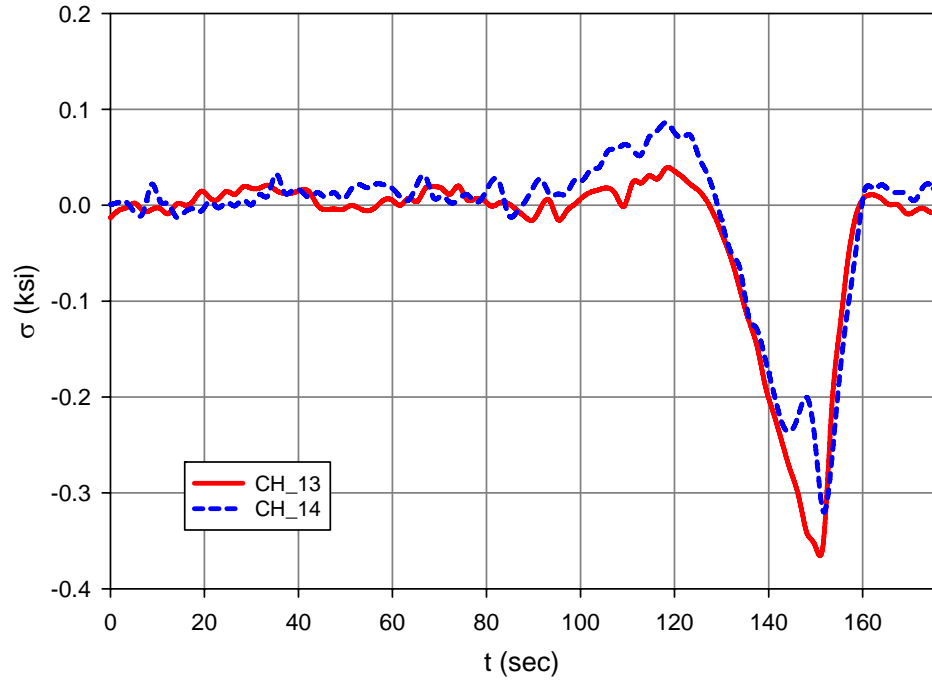
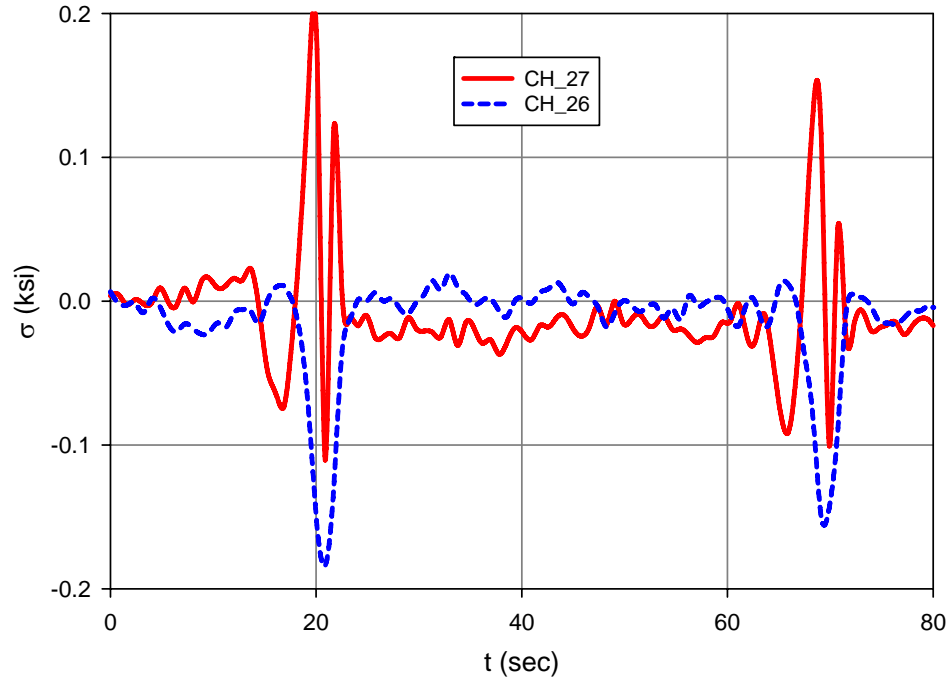**Figure 29** **Stresses measured at strain gage channels CH_13 and CH_14 during crawl load test CRWL_2**
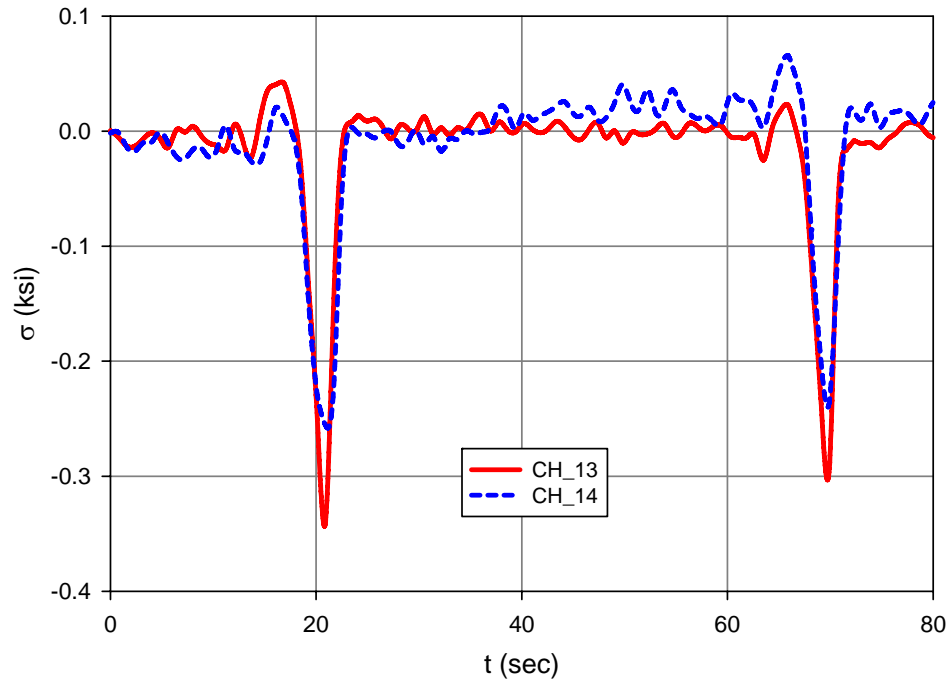
Figure 30 **Stresses measured at strain gage channels CH_13 and CH_14 during dynamic load test DYN_3**
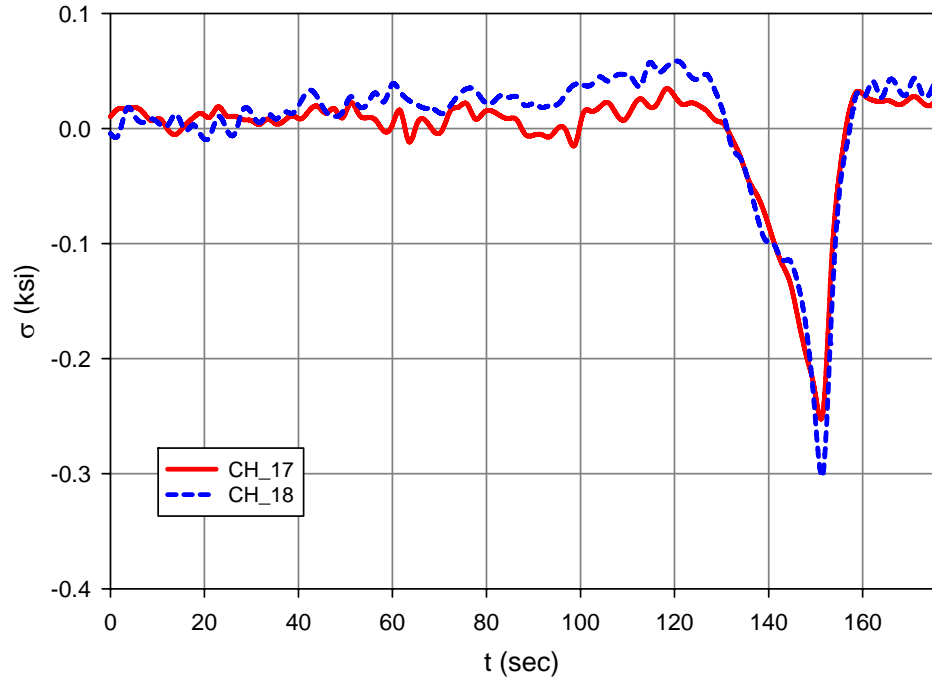
Figure 31 **Stresses measured at strain gage channels CH_17 and CH_18 during crawl load test CRWL_2**
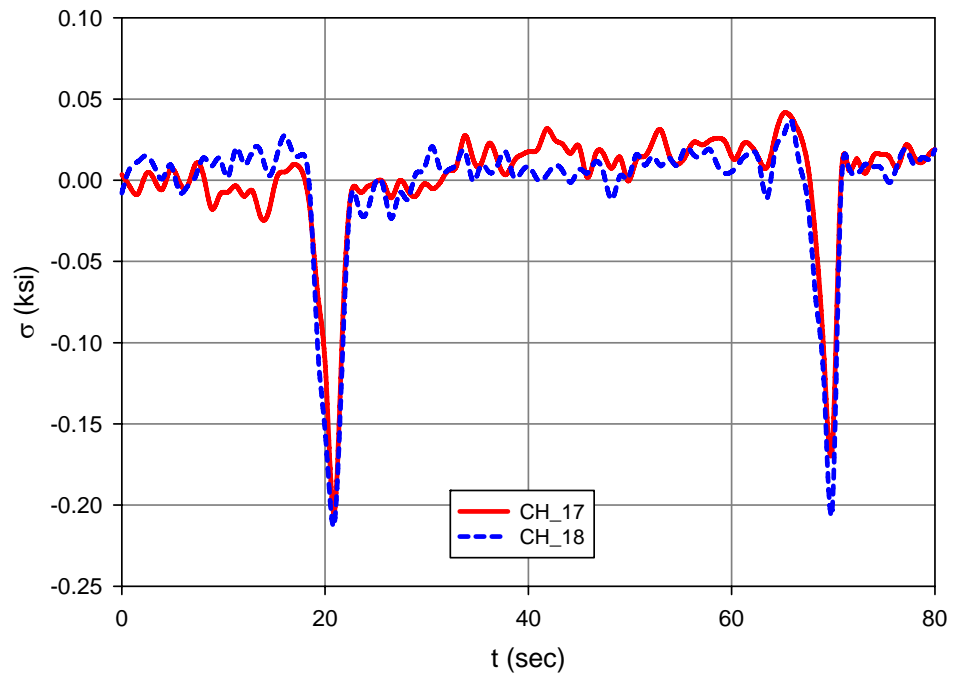
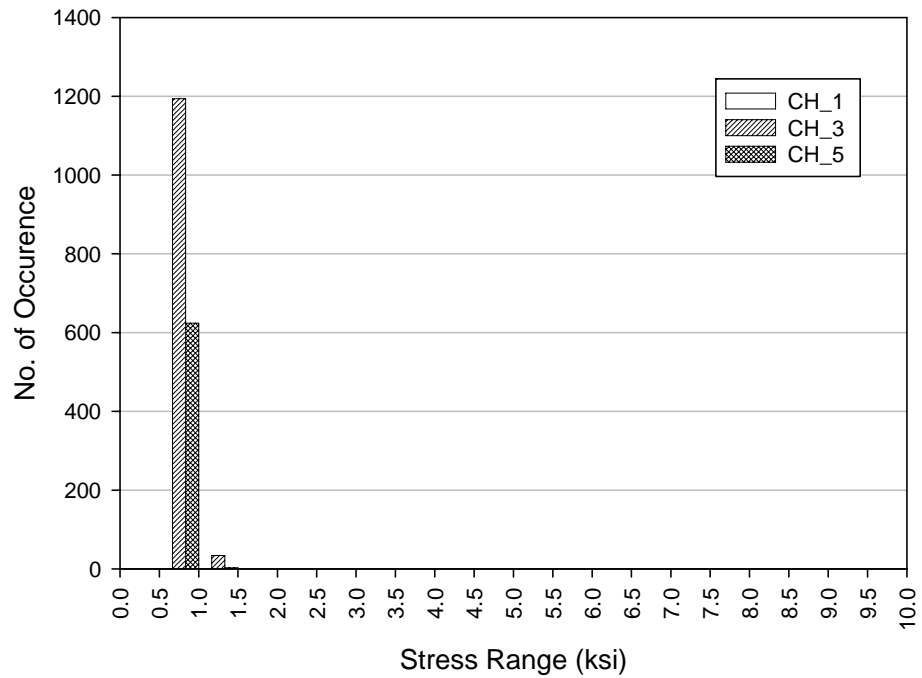**Figure 32** **Stresses measured at strain gage channels CH_17 and CH_18 during dynamic load test DYN_3**
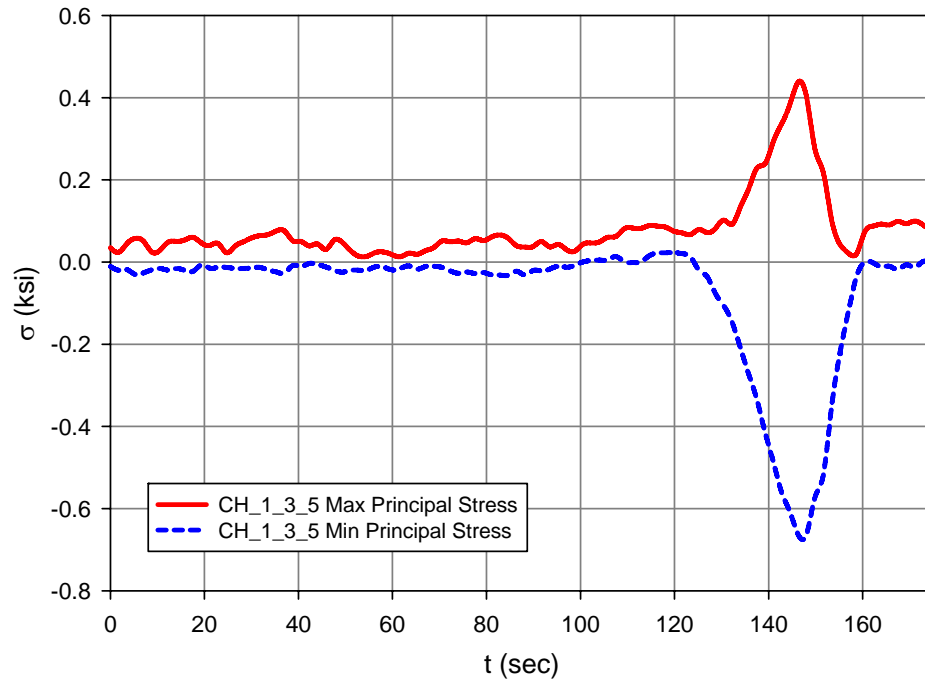
Figure 33   Measured principal stresses at strain rosette (CH_1, CH_3 and CH_5) during crawl load test CRWL_2
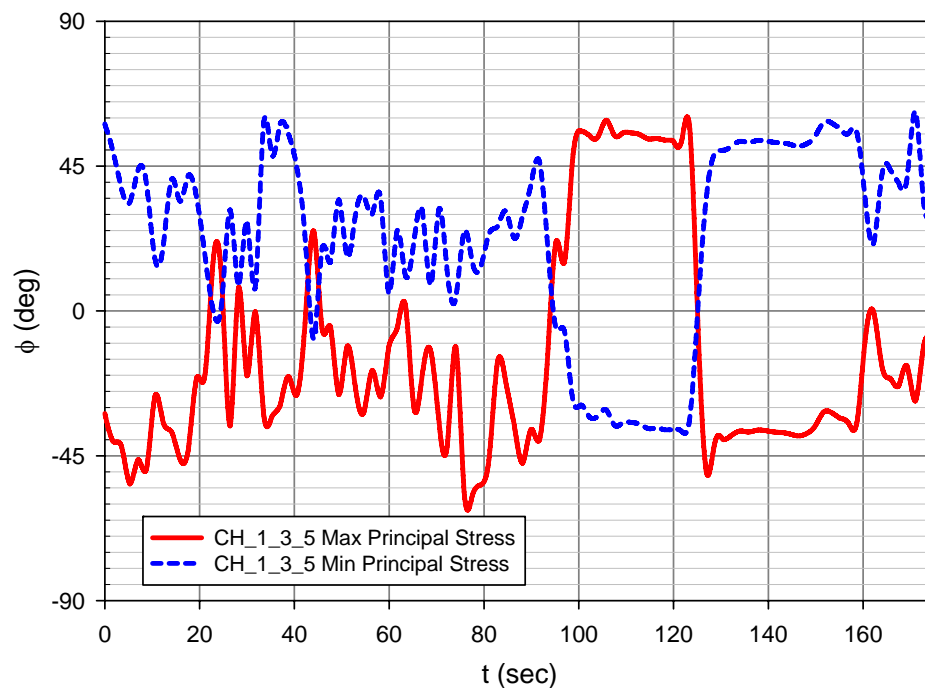
Figure 34   Direction of principal stresses at strain rosette (CH_1, CH_3 and CH_5) during crawl load test CRWL_2
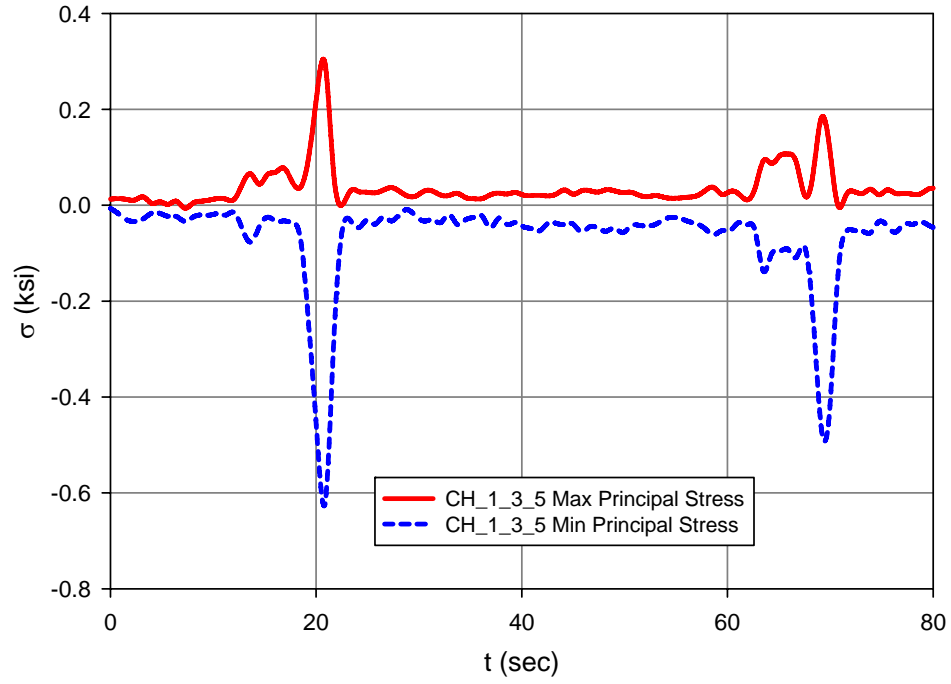
Figure 35 **Measured principal stresses at strain rosette (CH_1, CH_3 and CH_5) during dynamic load test DYN_3**
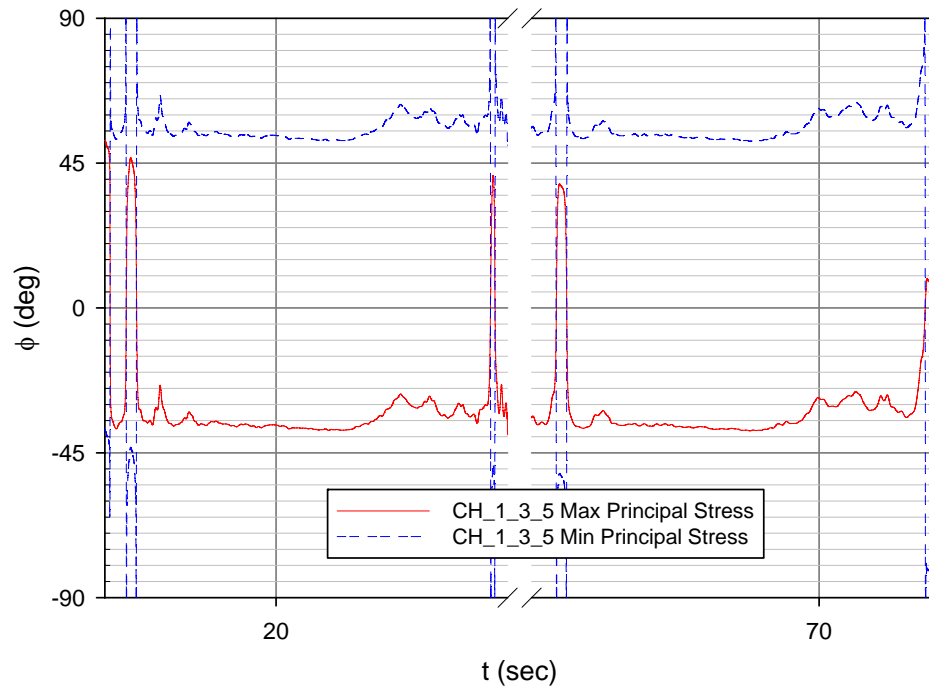
Figure 36 **Direction of principal stresses at strain rosette (CH_1, CH_3 and CH_5) during dynamic load test DYN_3**
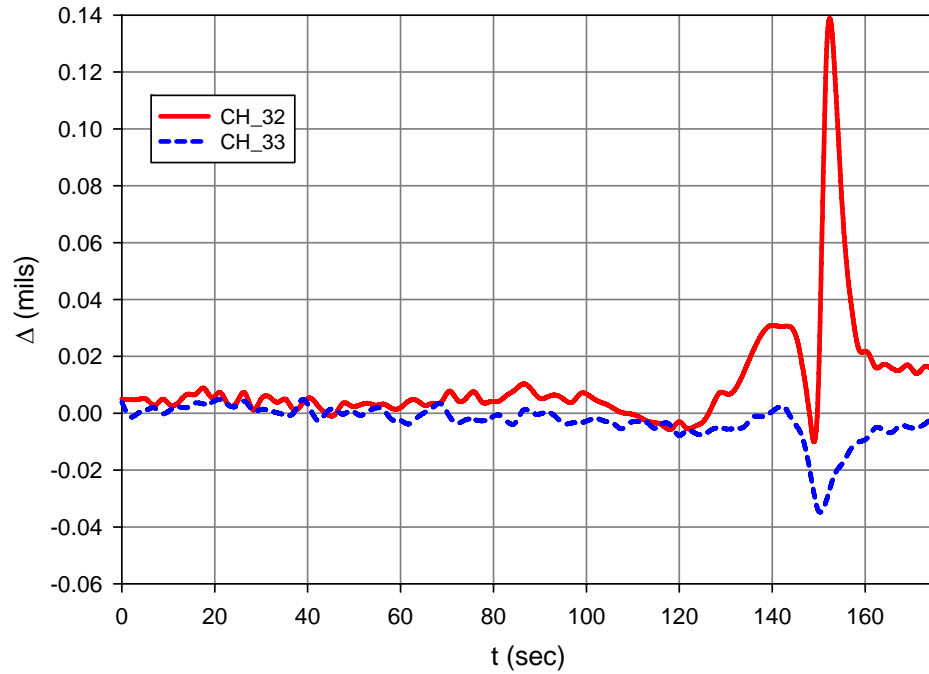
Figure 37   **Displacements measured at LVDT channels CH_32 and CH_33 during crawl load test CRWL_2**
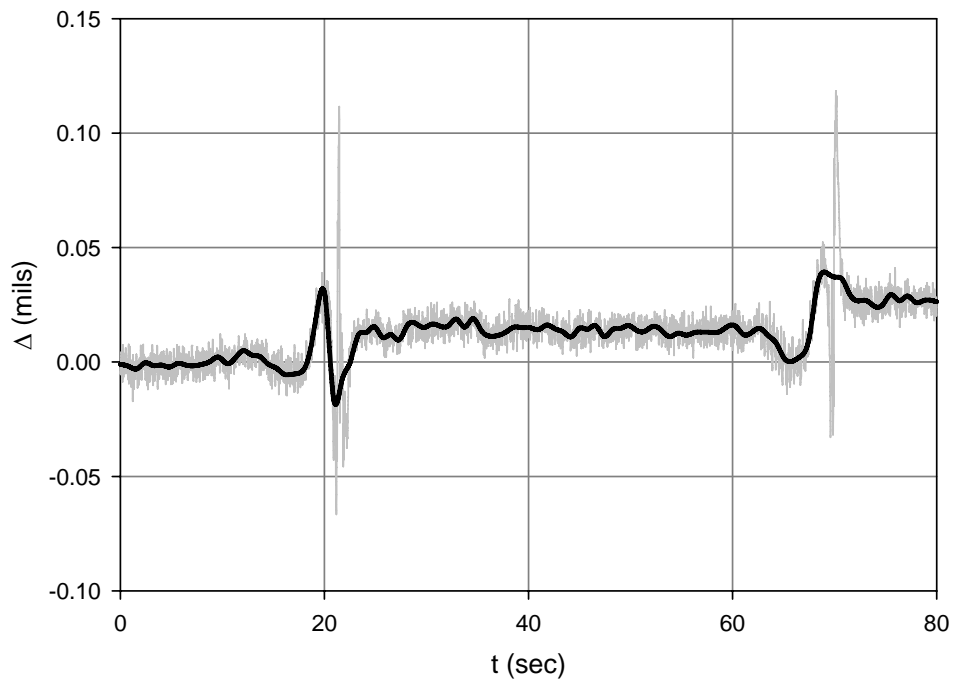
Figure 38   **Displacement measured at LVDT channel CH_32 during dynamic load test DYN_3**

41
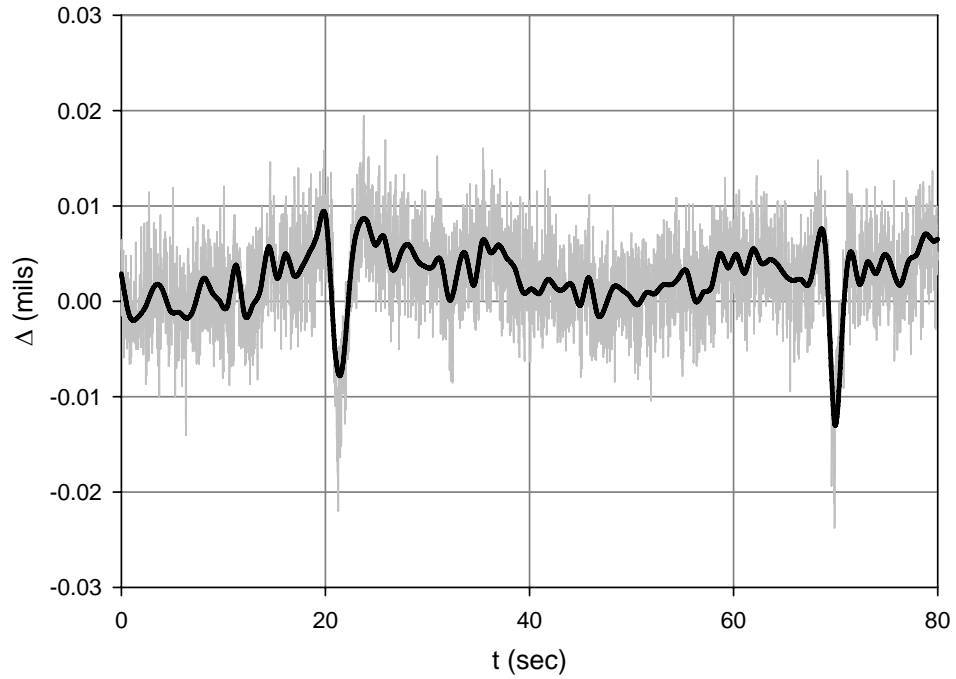
Figure 39 **Displacement measured at LVDT channel CH_33 during dynamic load test DYN_3**
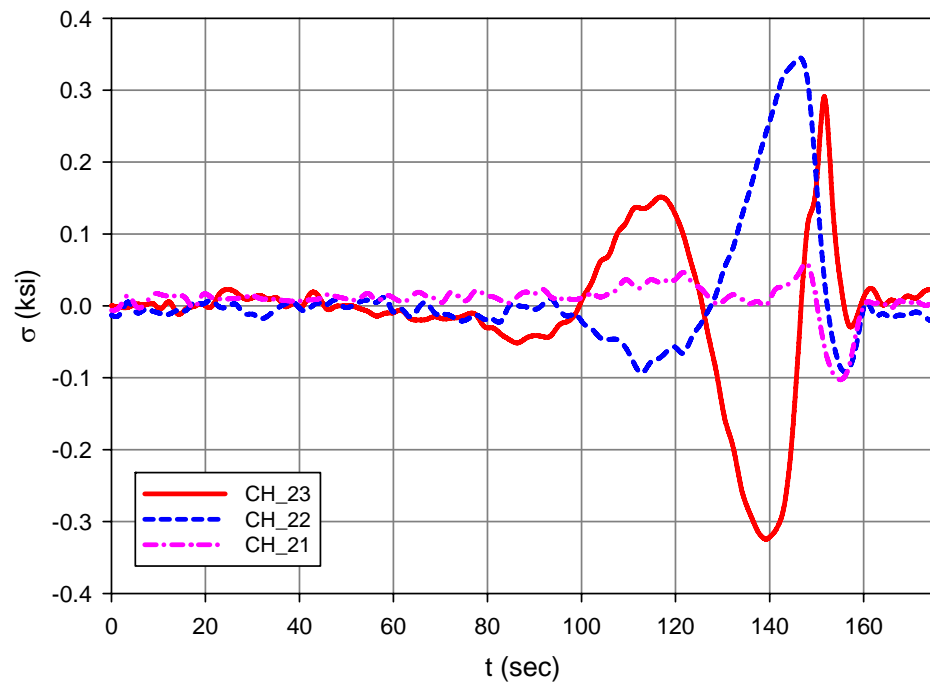
Figure 40 **Stresses measured at strain gage channels CH_21, CH_22 and CH_23 during crawl load test CRWL_2**
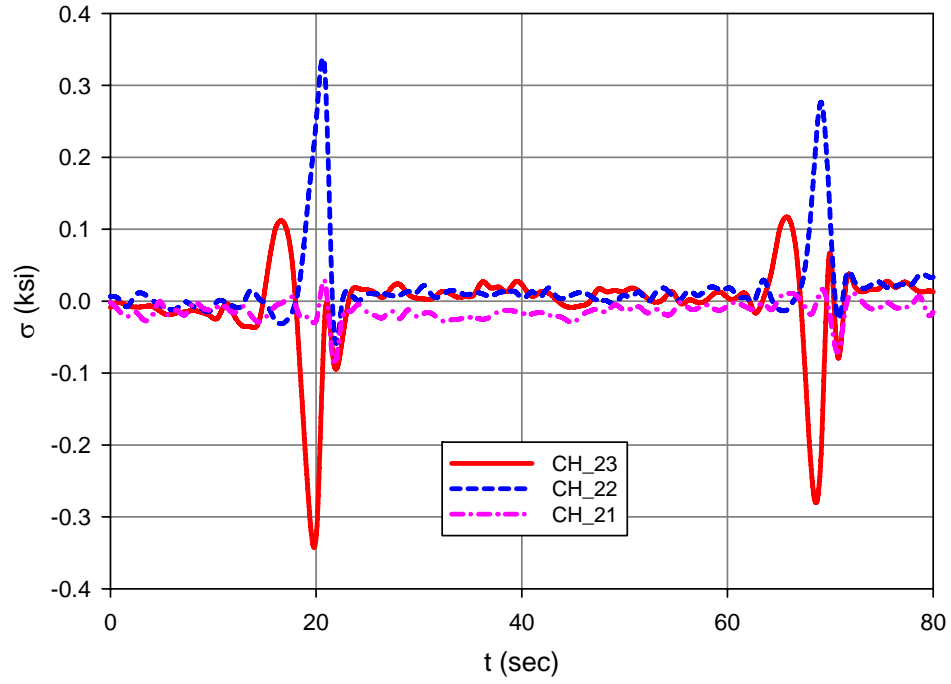
Figure 41   **Stresses measured at strain gage channels CH_21, CH_22 and CH_23 during dynamic load test DYN_3**
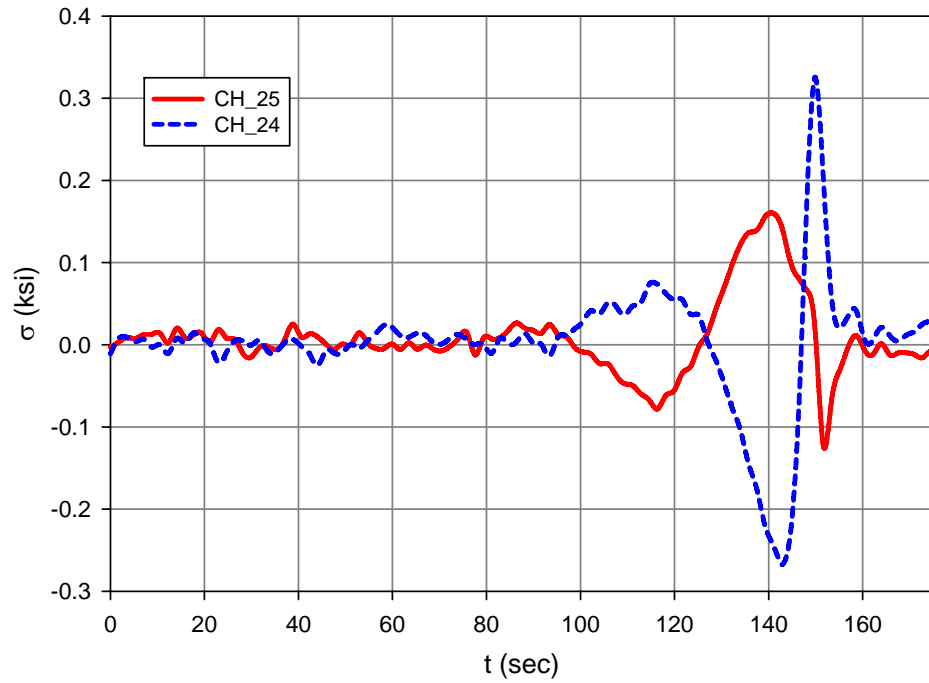
Figure 42   **Stresses measured at strain gage channels CH_24 and CH_25 during crawl load test CRWL_2**
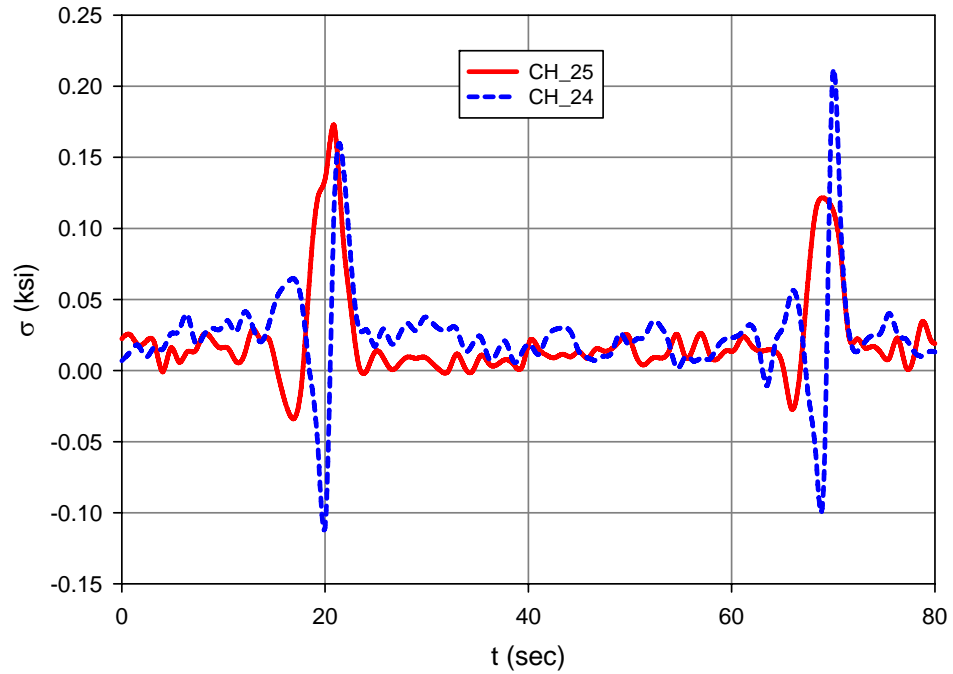
Figure 43   **Stresses measured at strain gage channels CH_24 and CH_25 during dynamic load test DYN_3**

Figure 44   **Stresses measured at strain gage channels CH_26 and CH_27 during crawl load test CRWL_2**

44

Figure 45   Stresses measured at strain gage channels CH_26 and CH_27 during dynamic load test DYN_3

Figure 46   Measured stress range histogram at strain gage channels CH_1, CH_3 and CH_5
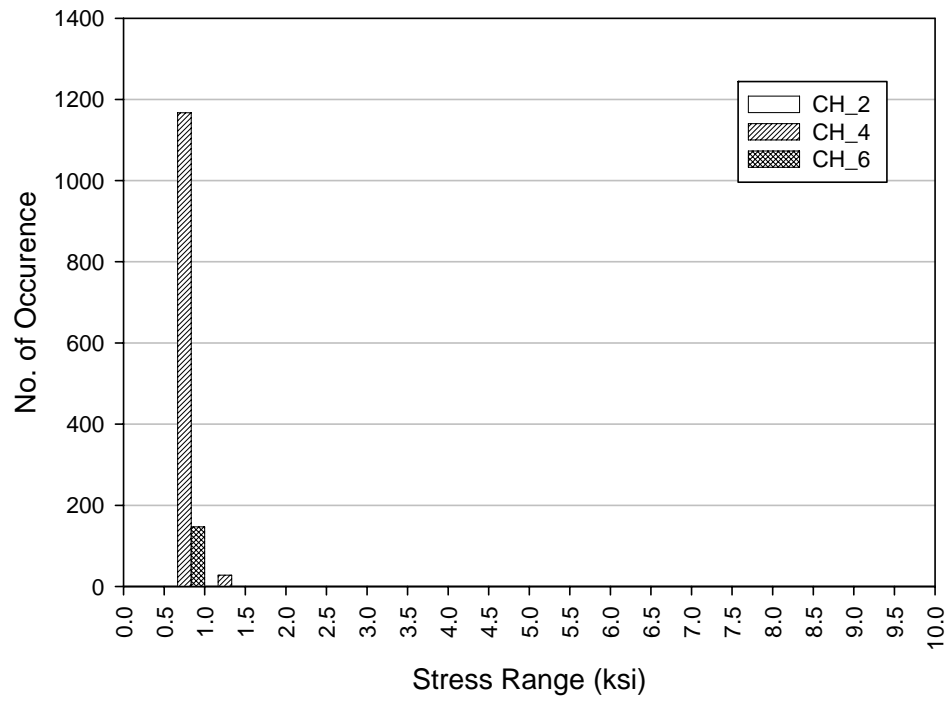
Figure 47   **Measured stress range histogram at strain gage channels CH_2, CH_4 and CH_6**
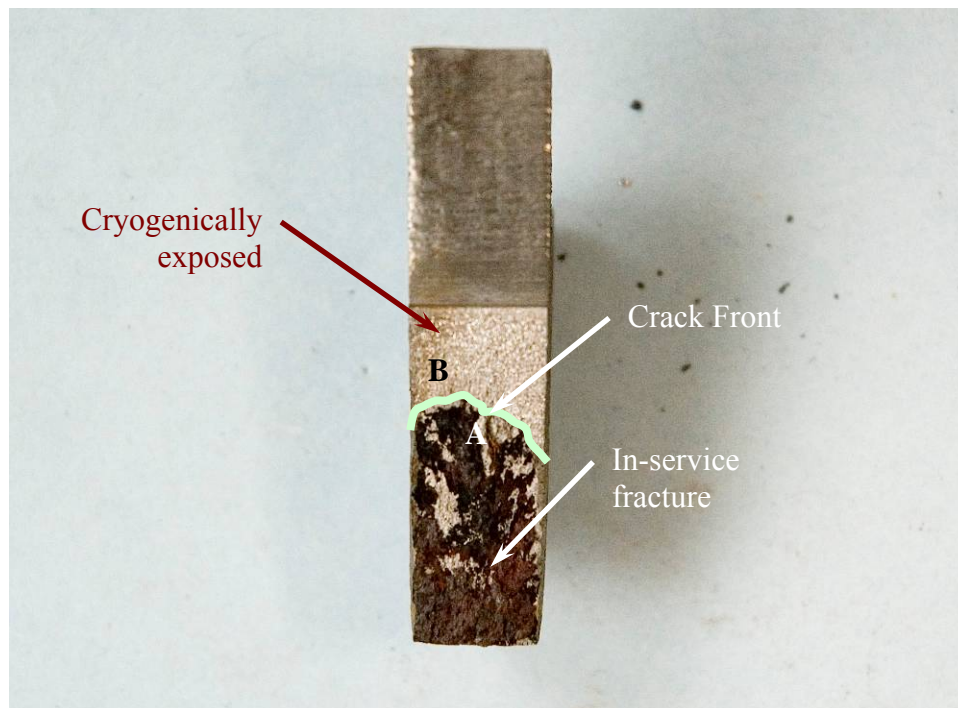
Figure 48   **Exposed surface of crack in web**

In-service fracture surface

A

B

9.0× 20.0 kV 1mm 29 mm CL:5.0
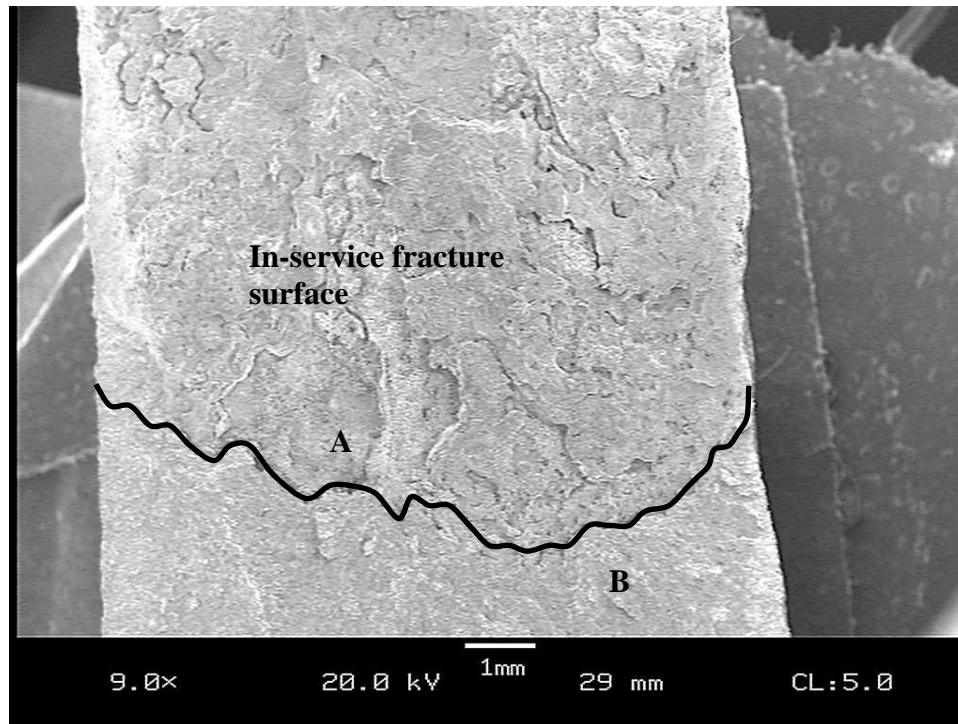
Figure 49 **Scanning Electron Micrograph of fracture surface near crack front, 9×**

404× 20.0 kV 100μm 29 mm CL:5.0
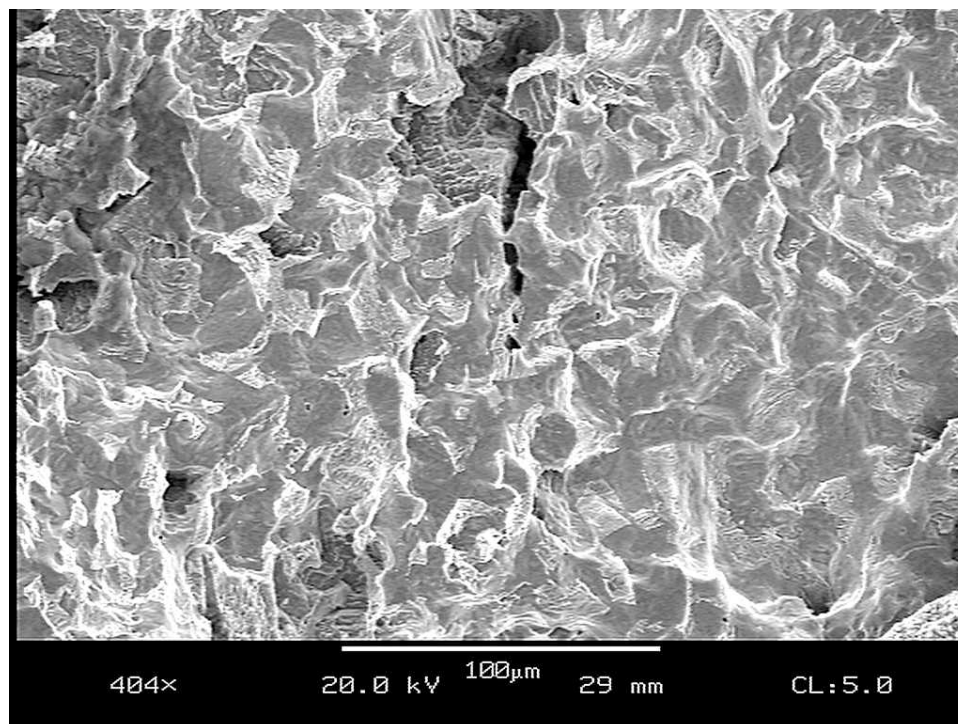
Figure 50 **Scanning Electron Micrograph of fracture surface near point A of Figure 49, 404×**

Figure 51   Attempt of drilling core to retrieve possible crack origin

Existing holes
drilled at crack tip

$4\frac{1}{2}$ "

Cut piece for material test

1"

Drill 2" Ø core
as close to the bearing
stiffener as possible
including both cracks

Crack

7"

All cut edges shall be ground smooth
and the sharp corners shall be rounded

G3
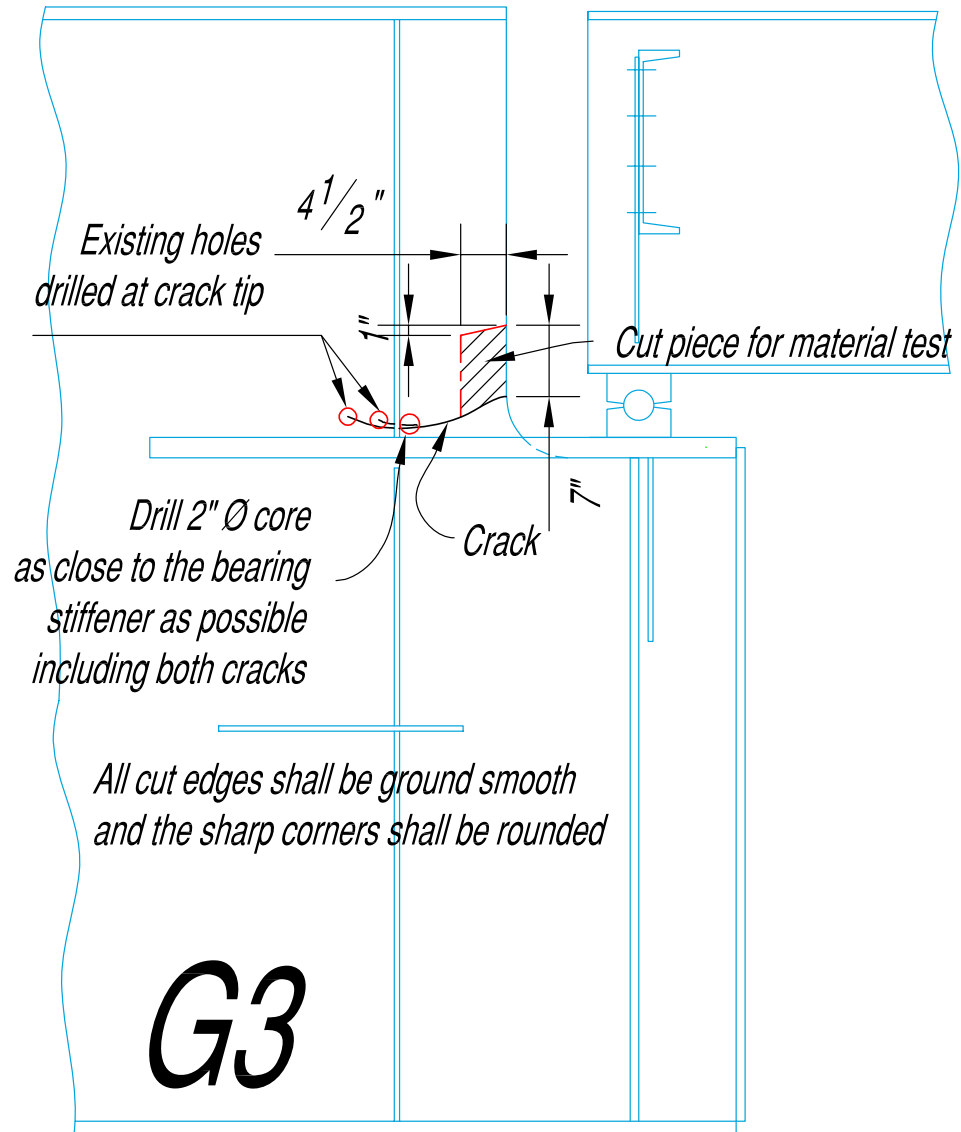
Figure 52   **Cut piece of girder web used for material test**

3# CVN Specimens (TYP.)

9# CVN Specimens (TYP.)

3.0"

2 # Ø.252 Tensile Specimens (3" long)
$^{3}/_{8}$ -16 thread
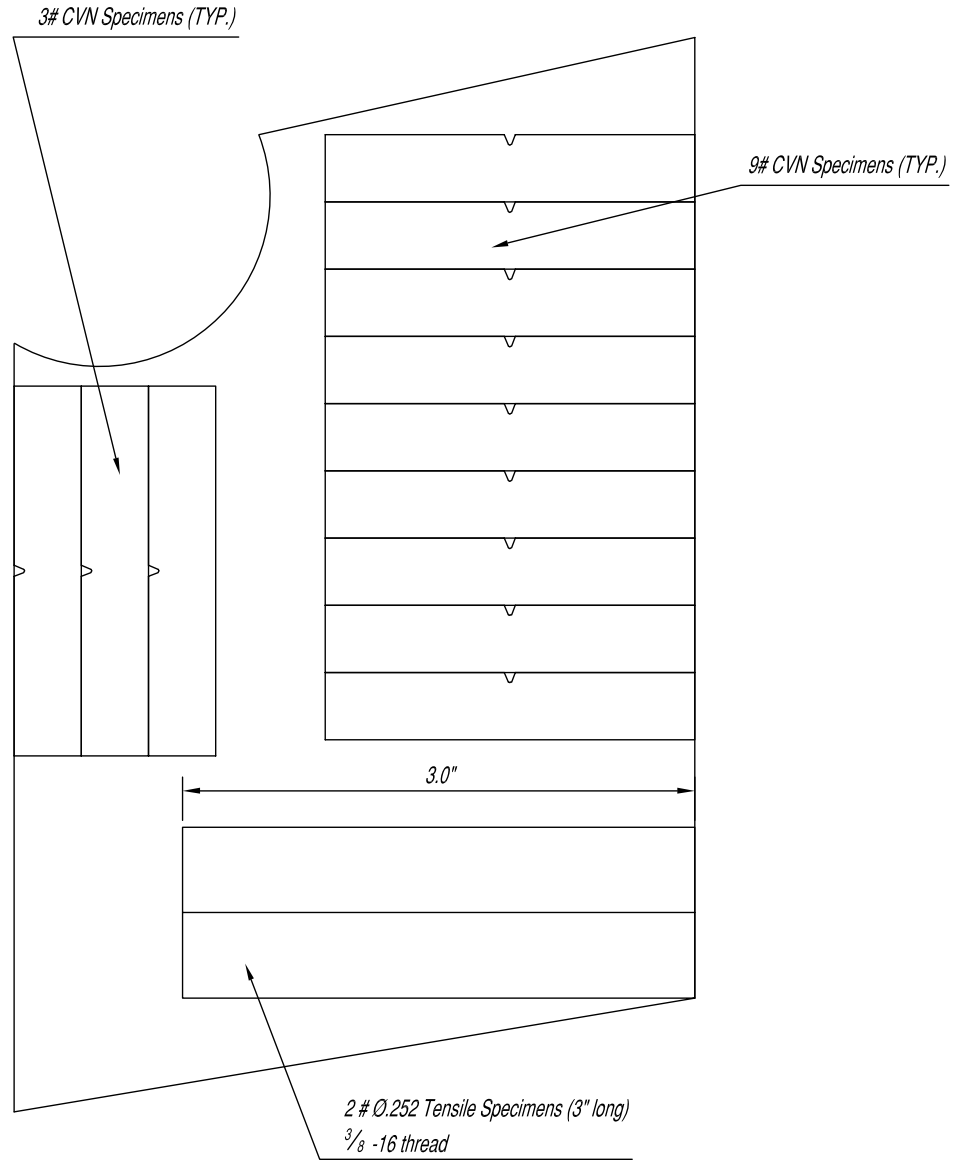
Figure 53   Cutting plan of specimens for material test
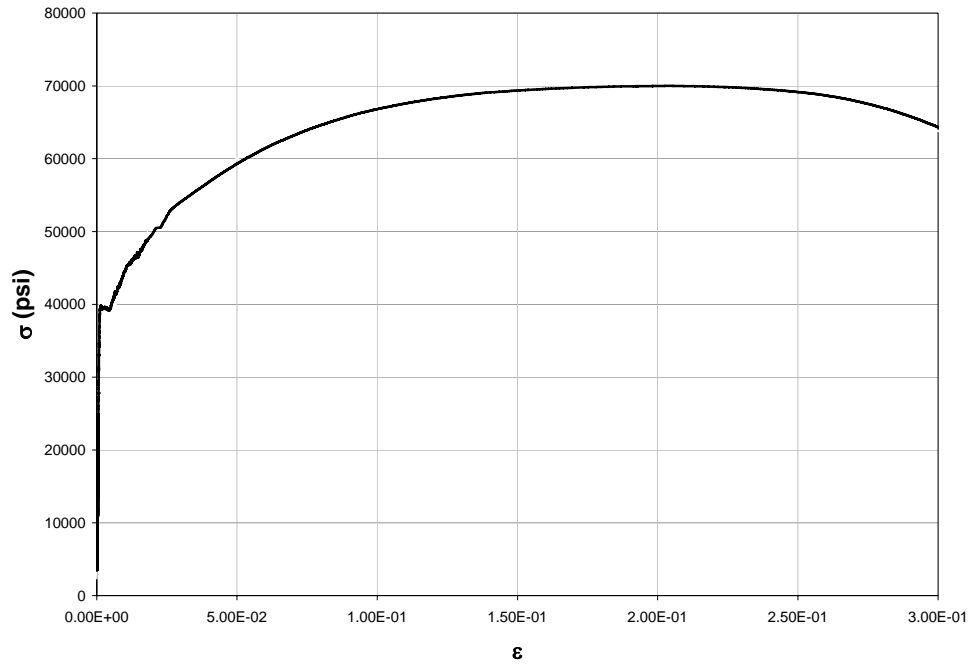
Figure 54   **Stress strain response of web steel: Specimen I**
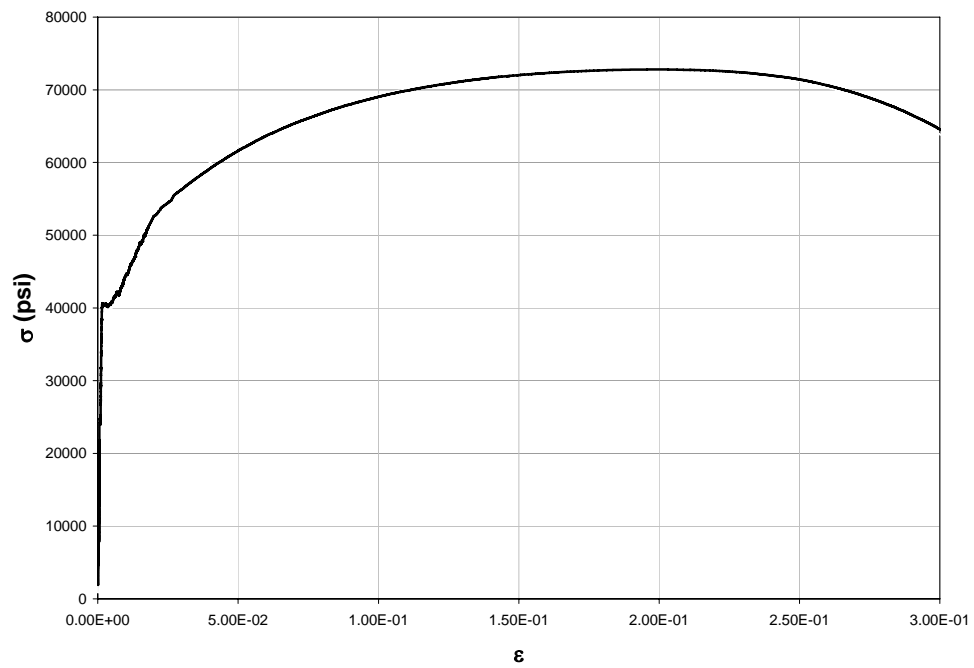
Figure 55   **Stress strain response of web steel: Specimen II**
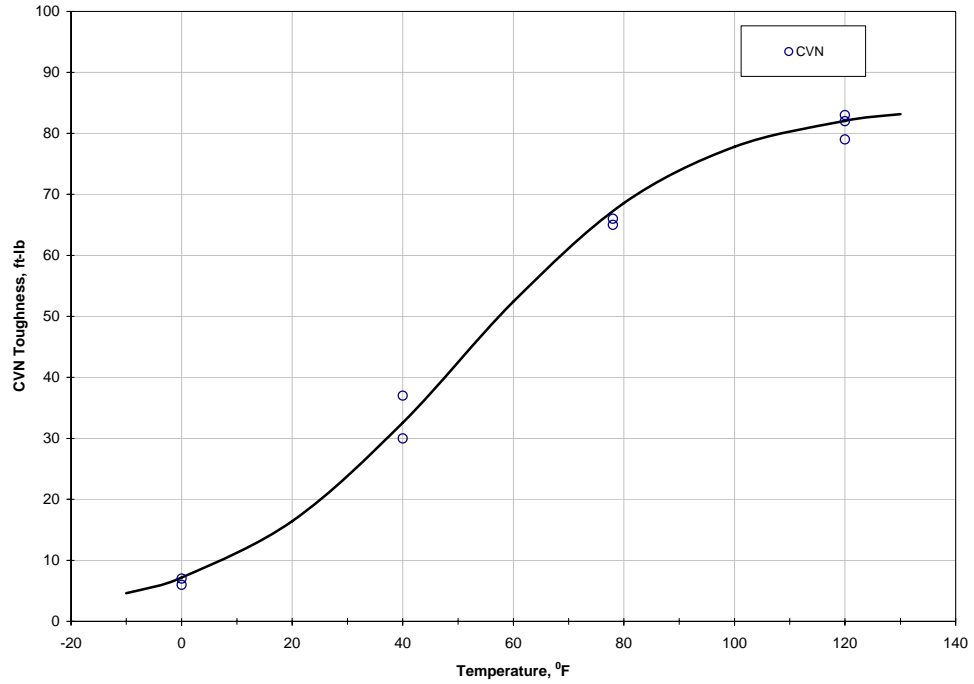
Figure 56   Charpy V Notch toughness of web steel: longitudinal
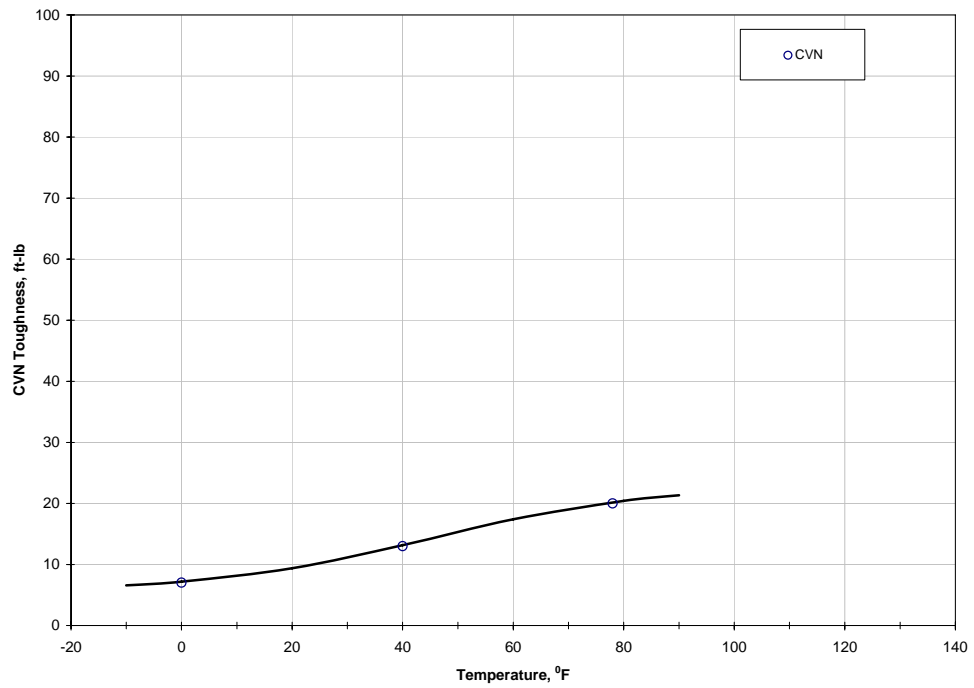
Figure 57   Charpy V Notch toughness of web steel: transverse
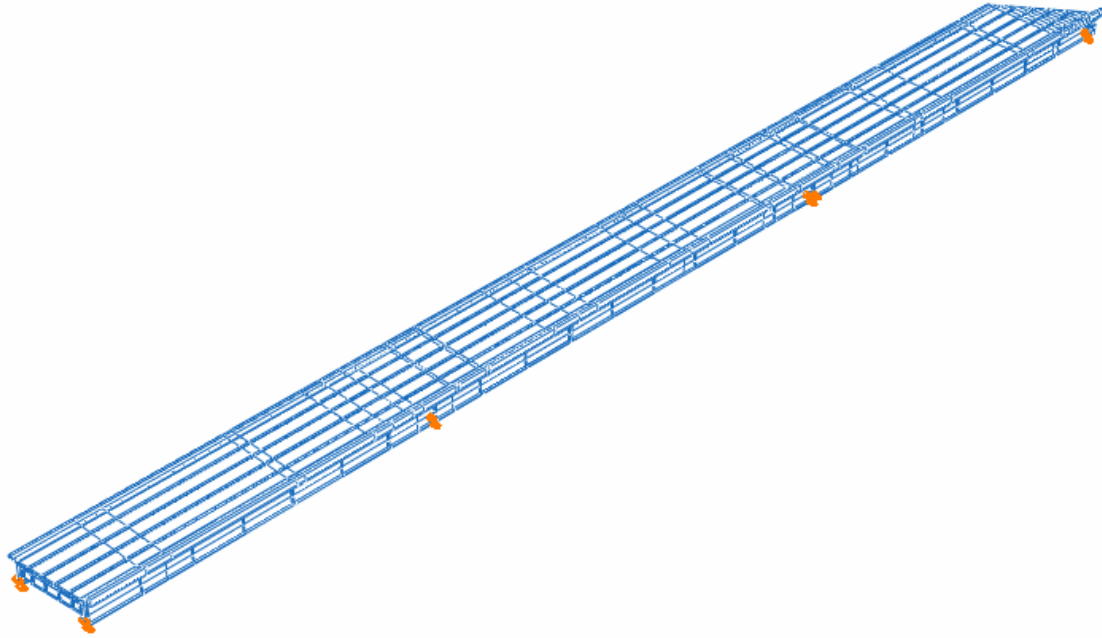
Figure 58   FE model: overall bridge viewing East
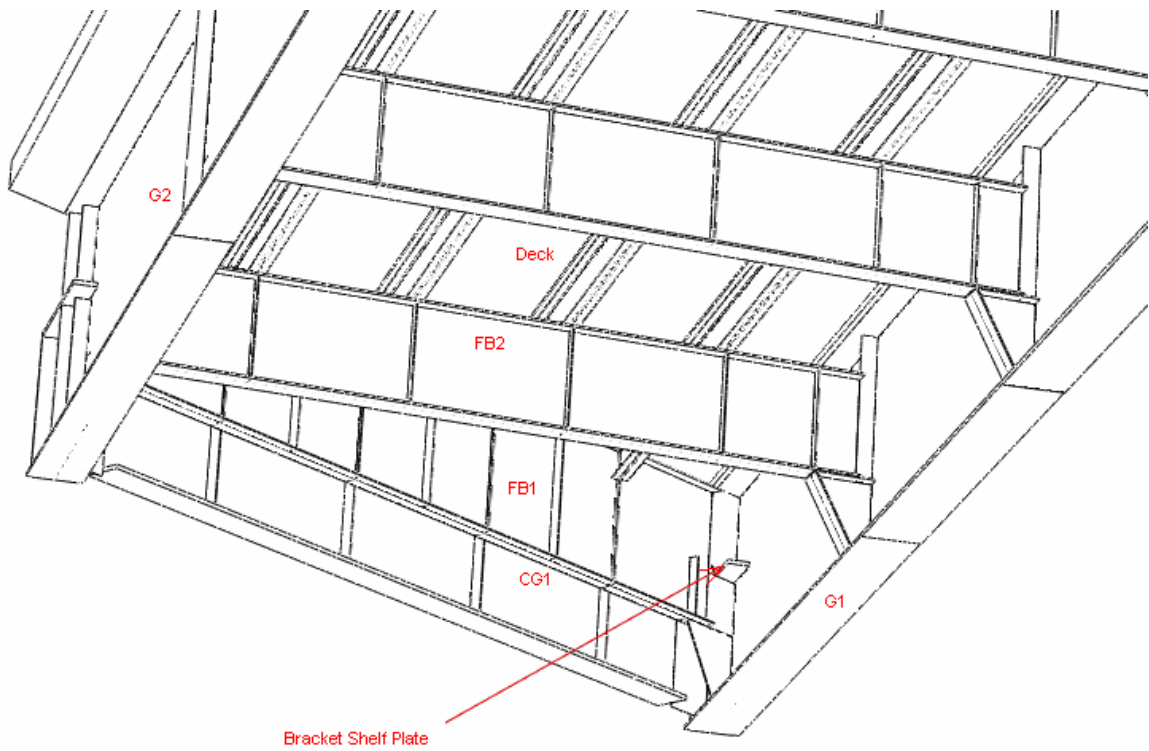
Figure 59   FE model: underside of the bridge
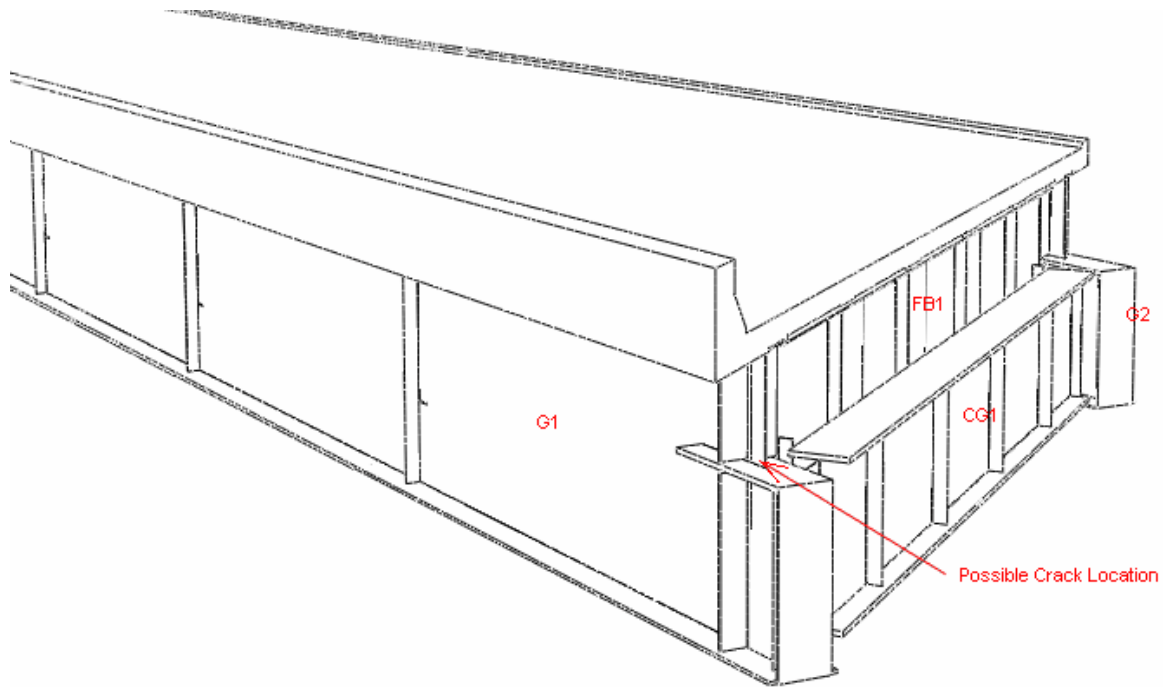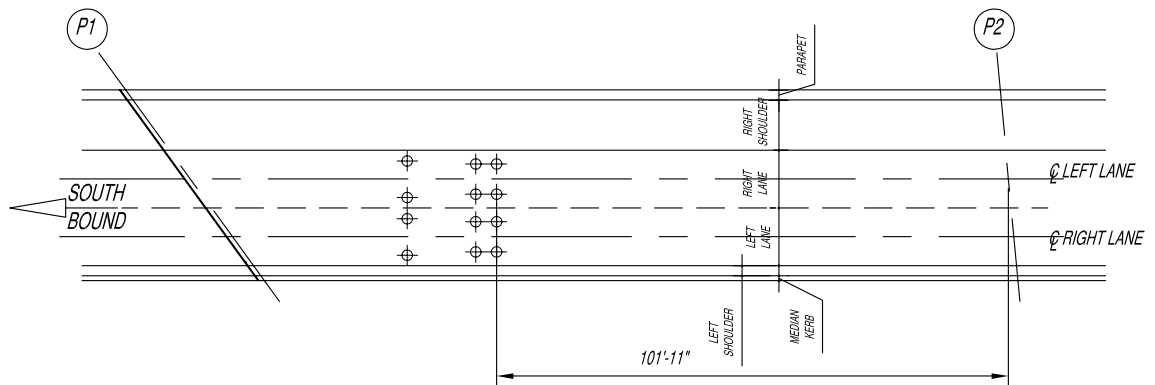
Figure 60   FE model: South-West view of the bridge

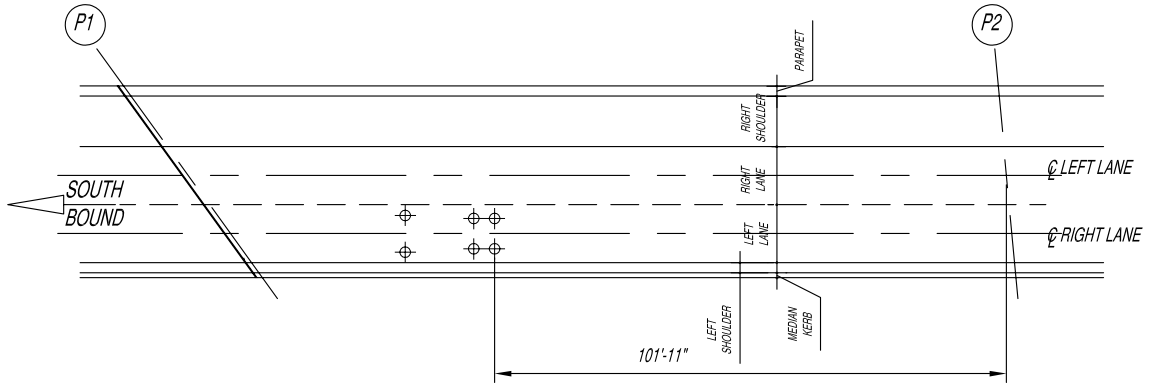**Figure 61   Wheel load disposition in Load Case 1 – controlled load test CRWL_2**

54

Figure 62   **Wheel load disposition in Load Case 2 – controlled load test CRWL_1 left lane loaded**
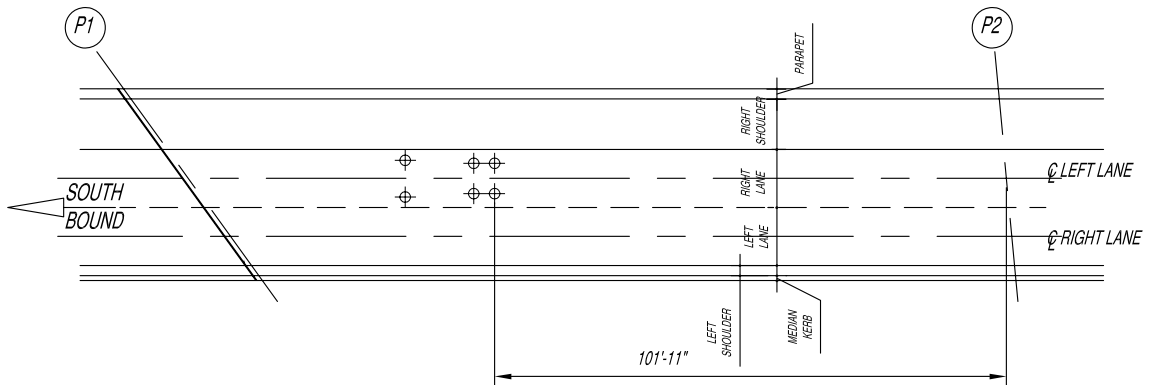

Figure 63   **Wheel load disposition in Load Case 3 – controlled load test CRWL_1 right lane loaded**
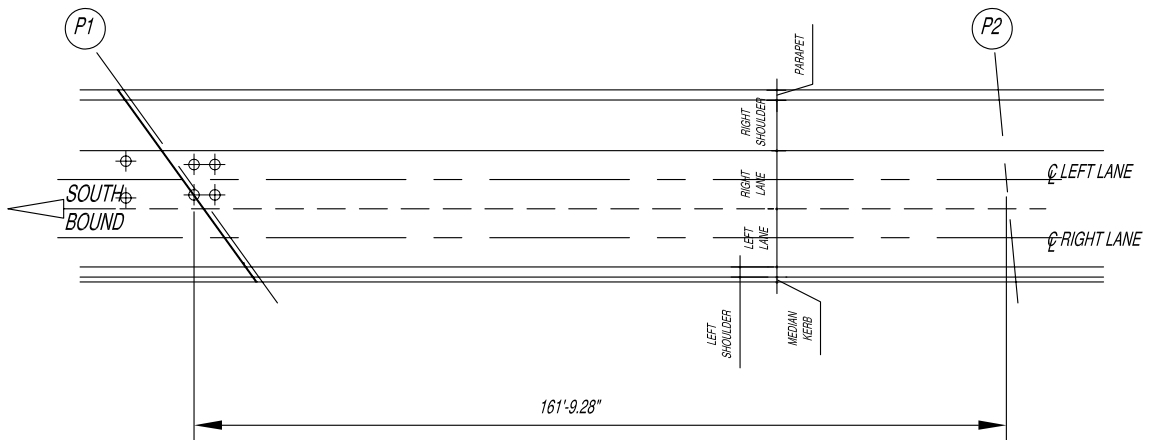

Figure 64   **Wheel load disposition in Load Case 4 – controlled load test CRWL_1 right lane loaded over near bearing stiffener at Pier 1**
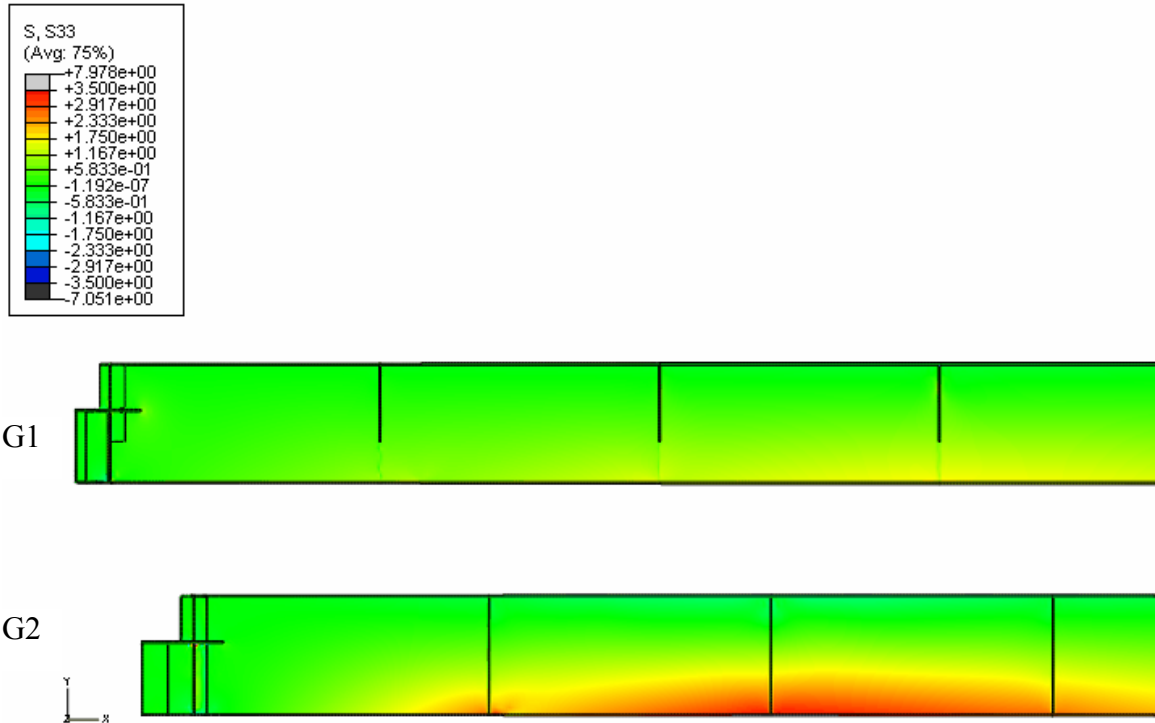
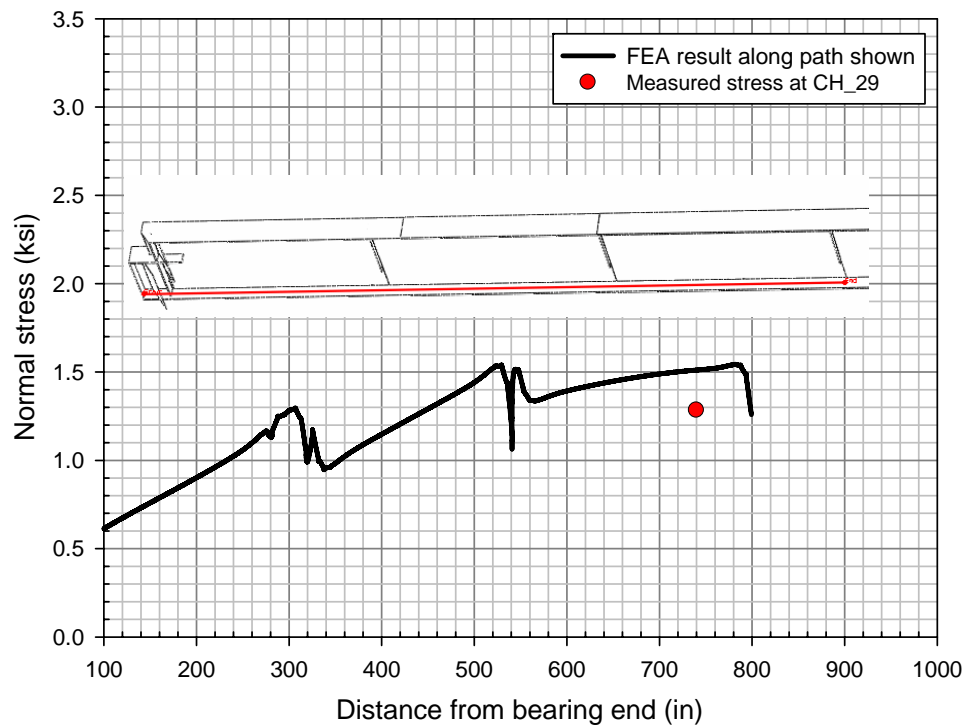**Figure 65**   **FEA result – Load Case 1: Longitudinal stress in Girders G1 and G2**

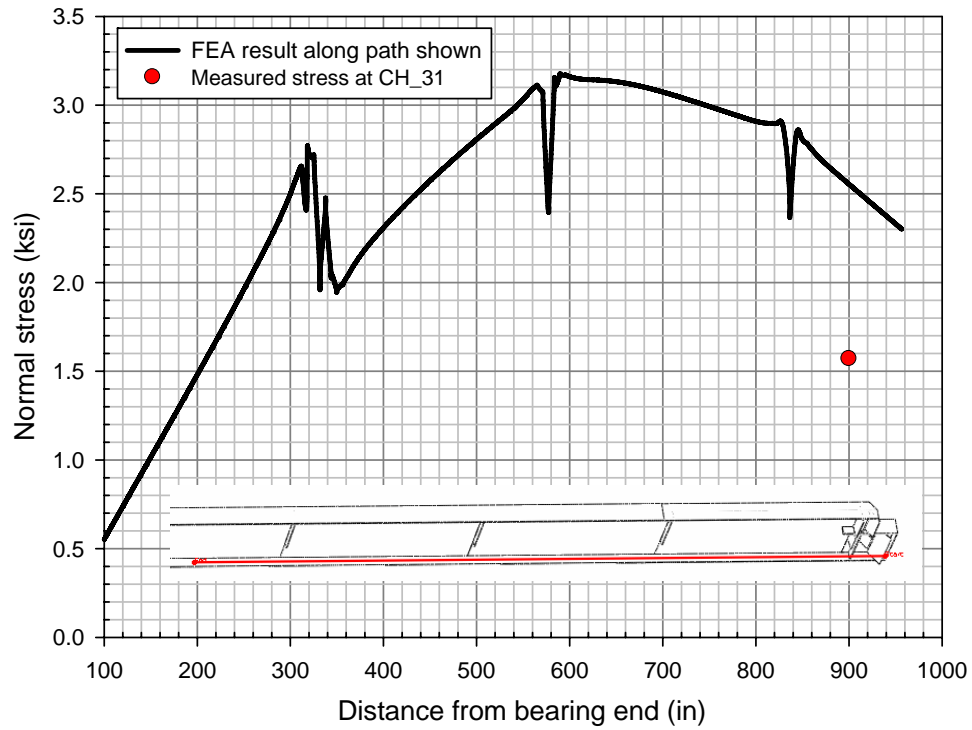**Figure 66**   **Inner face stress at bottom flange of Girder G1: FEA result vs. measurement – load test CRWL_2**

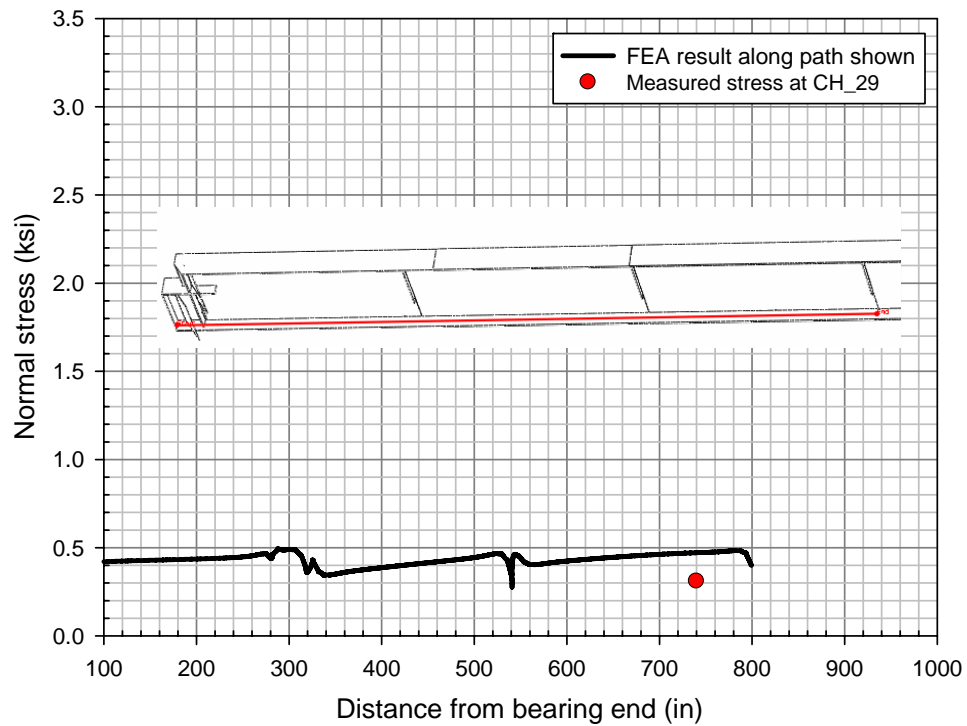**Figure 67** **Inner face stress at bottom flange of Girder G2: FEA result vs. measurement – load test CRWL_2**

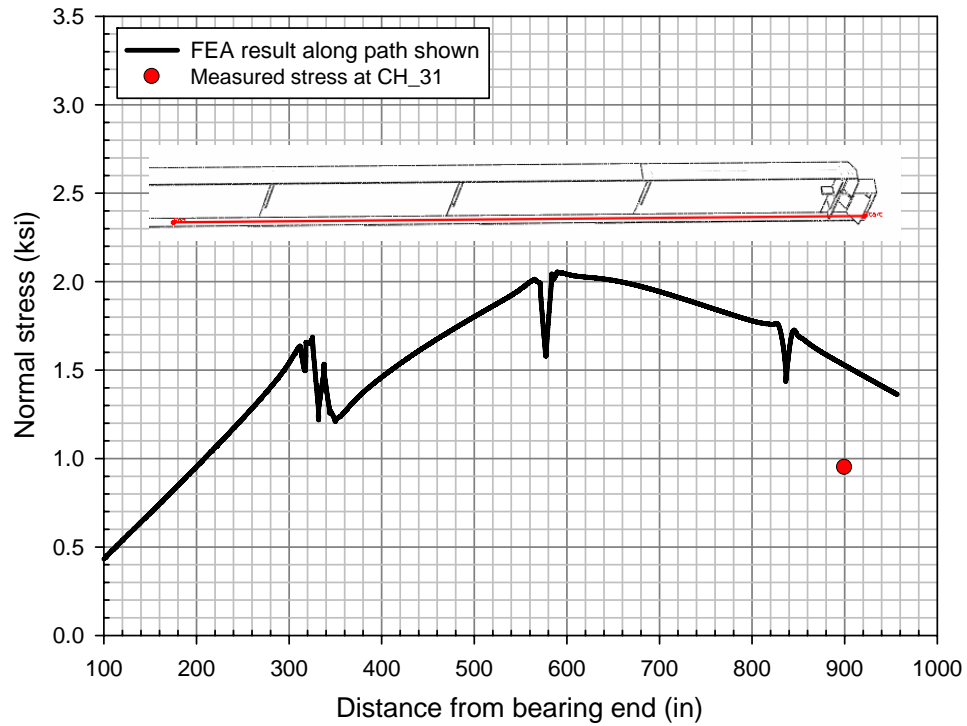**Figure 68** **Inner face stress at bottom flange of Girder G1: FEA result vs. measurement – load test CRWL_1 left lane**

Figure 69   **Inner face stress at bottom flange of Girder G2: FEA result vs. measurement – load test CRWL_1 left lane**
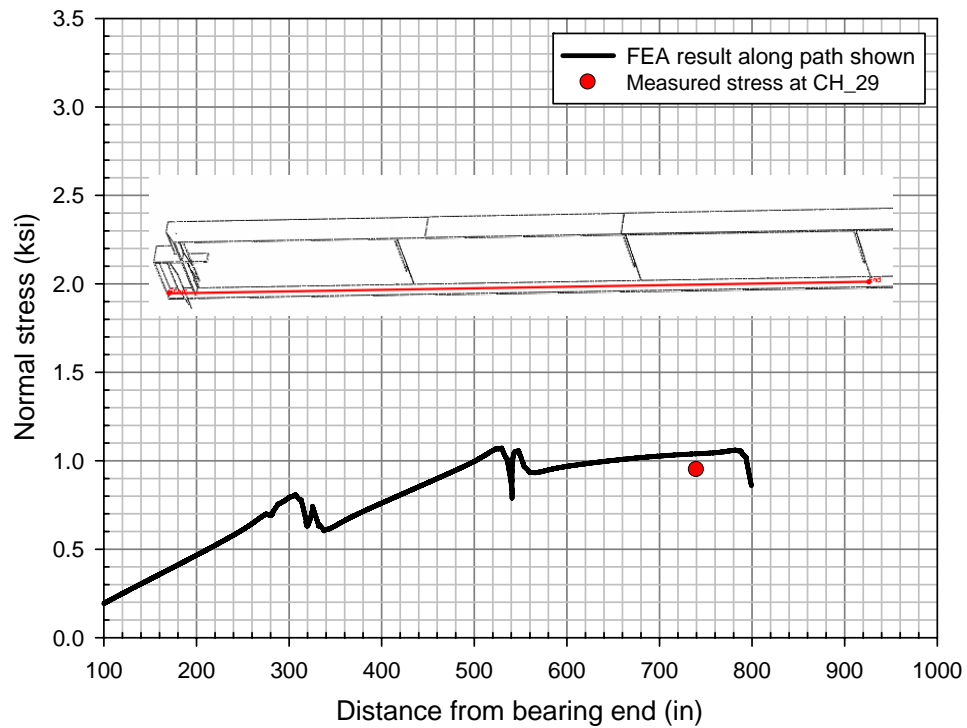

Figure 70   **Inner face stress at bottom flange of Girder G1: FEA result vs. measurement – load test CRWL_1 right lane**
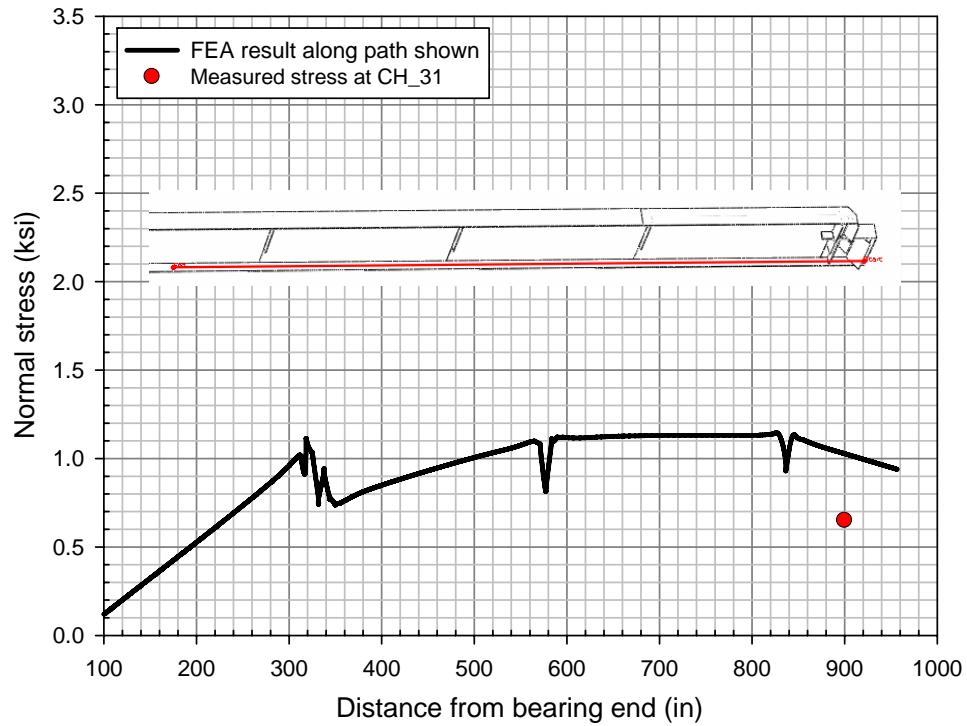
Figure 71 **Inner face stress at bottom flange of Girder G2: FEA result vs. measurement – load test CRWL_1 right lane**

Figure 72 **Principal stress field near the bearing stiffener / connection plate web gap in Girder G1 at Pier 1 (outer face) – controlled load test CRWL_1 right lane loaded**
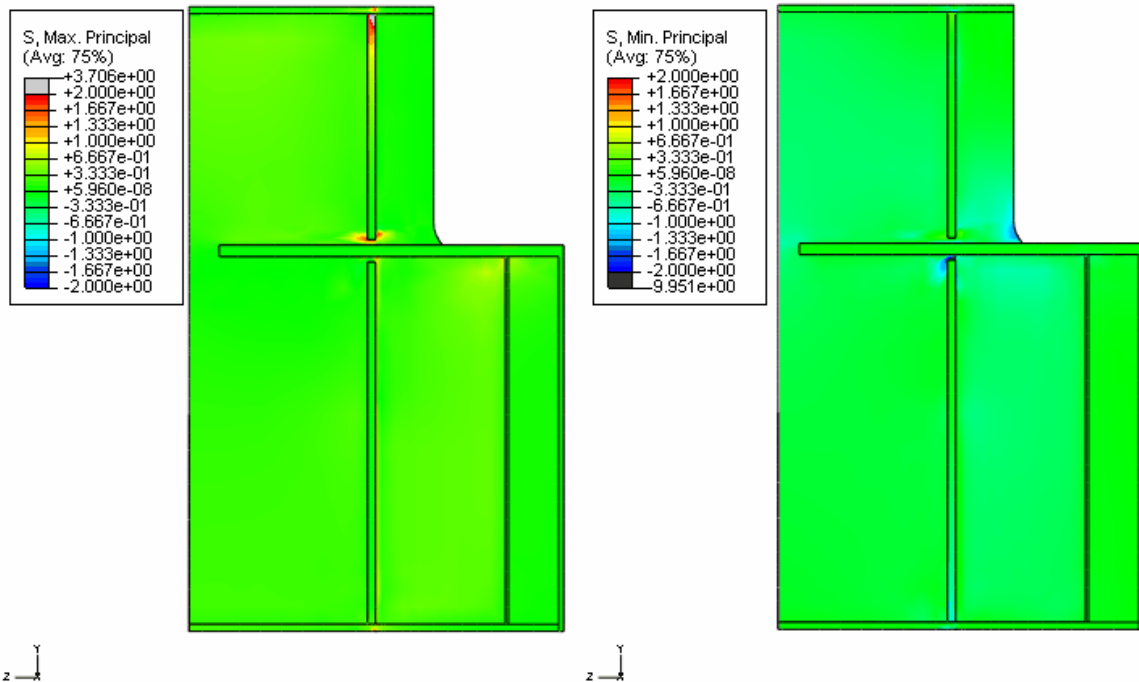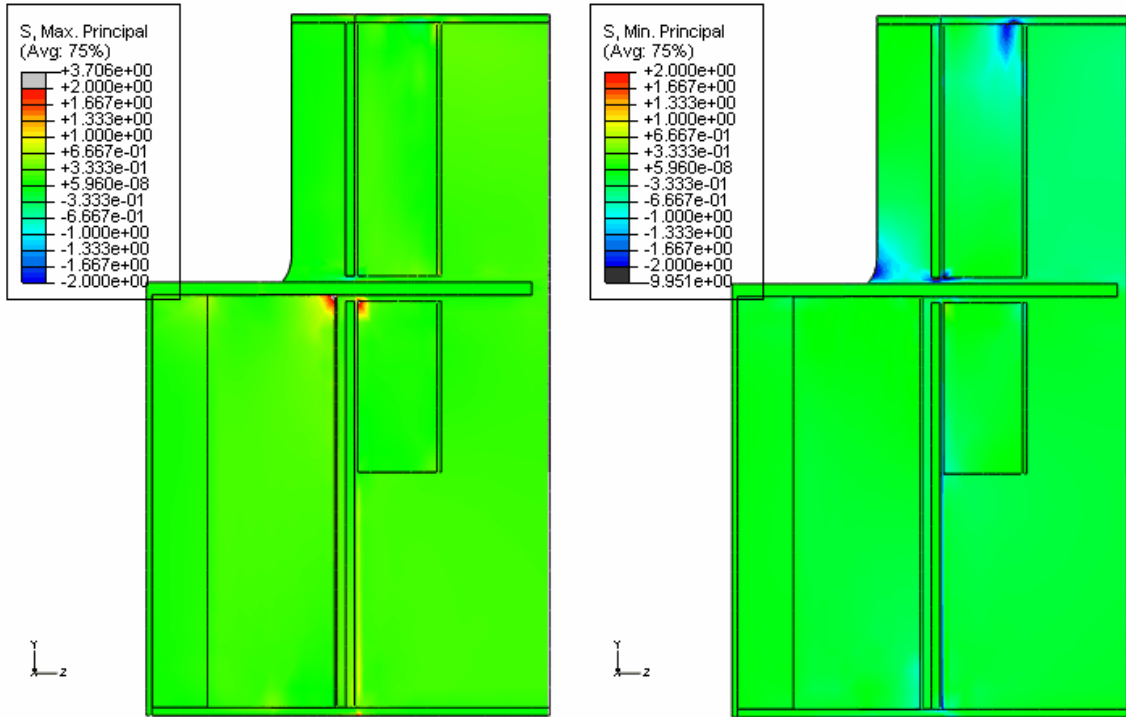
Figure 73 **Principal stress field near the bearing stiffener / connection plate web gap in Girder G1 at Pier 1 (inner face) – controlled load test CRWL_1 right lane loaded**

REFERENCES

Load Case 1 – PennDOT District 6-0 NBIS Inspection: Montgomery County. DMJM HARRIS, 2005

Load Case 2 – Email Communiations between Edwards & Kelcey and Lehigh University, 2006

APPENDIX A   LOAD TEST RESULTS

The time history plots of measured data at all channels and for all the controlled load tests are included in attached CD ROM.

APPENDIX B   CHEMICAL ANALYSIS OF WEB STEEL

LABORATORY TESTING INC.

Certified Test Report

LHU001-07-01-02417-1

Nadcap
pri
PERFORMANCE
REVIEW INSTITUTE
• Accredited •
ISO/IEC 17025
Materials Testing Laboratory
NDT (PT, MT, UT)

2331 Topaz Drive, Hatfield, PA 19440
TEL: 800-219-9095 • FAX: 800-219-9096

SOLD TO
Lehigh University
ATLSS Eng. Research Center
117 ATLSS Drive, Bldg. H
Bethlehem, PA 18015
CUSTOMER P.O.
69340

SHIP TO
Lehigh University
117 ATLSS Drive
Bethlehem, PA 18015-
ATTN: Eric Kaufman
CERTIFICATION DATE
2/9/2007
DESCRIPTION
1 pc.   Test Sample

SHIP VIA
EMAIL & LTI DEL

*AMENDED CERTIFICATION (2/27/07)
The submitted sample was analyzed in accordance with Customer's Instructions with the following results:

ELEMENT	ACTUAL
Al	0.008%
B	0.0003%
Bi	0.006%
C	0.219%
Ca	0.0004%
Co	0.005%
Cr	0.039%
Cu	0.034%
Mn	0.750%
Mo	0.006%
N	0.005%
*Nb	<0.001%
Ni	0.044%
P	0.009%
S	0.019%
Si	0.049%
Sn	0.003%
Ta	0.018%
V	0.003%
W	0.019%

Procedures/Methods: 86-SCA-0, Rev. 7, Direct Reading Atom Emissions Spectroscopy

The services performed above were done in accordance with LTI's Quality System Program Manual Revision 17 dated 12/3/04 and ISO/IEC 17025. These results relate only to the items tested and this report shall not be reproduced, except in full, without the written approval of Laboratory Testing, Inc. L.T.I. is accredited by NADCAP to ISO/IEC 17025, Material's Testing and NDT (MT, PT and UT). Reported results represent the actual attributes of the material / item tested. Testing was performed in accordance with all applicable specification and contract / purchase order requirements.

MERCURY CONTAMINATION: During the testing and inspection, the product did not come in direct contact with mercury or any of its compounds nor with any mercury containing devices employing a single boundary of containment.

NOTE: The recording of false, fictitious or fraudulent statements or entries on this document may be punished as a felony under Federal Statutes.

Sherri L. Scheifele
QA Specialist

Sherri L. Scheifele

By: _____
Authorized Signature

Page 1 of 1